UNIVERSITY OF AMSTERDAM

UvA-DARE (Digital Academic Repository)

Exploiting large-pore metal-organic frameworks for separations through entropic molecular mechanisms

Torres-Knoop, A.; Dubbeldam, D.

DOI
10.1002/cphc.201500195

Publication date
2015

Document Version
Final published version

Published in
ChemPhysChem

License
Article 25fa Dutch Copyright Act

Link to publication

Citation for published version (APA):
Torres-Knoop, A., & Dubbeldam, D. (2015). Exploiting large-pore metal-organic frameworks for separations through entropic molecular mechanisms. *ChemPhysChem*, *16*(10), 2046-2067. https://doi.org/10.1002/cphc.201500195

General rights
It is not permitted to download or to forward/distribute the text or part of it without the consent of the author(s) and/or copyright holder(s), other than for strictly personal, individual use, unless the work is under an open content license (like Creative Commons).

Disclaimer/Complaints regulations
If you believe that digital publication of certain material infringes any of your rights or (privacy) interests, please let the Library know, stating your reasons. In case of a legitimate complaint, the Library will make the material inaccessible and/or remove it from the website. Please Ask the Library: https://uba.uva.nl/en/contact, or a letter to: Library of the University of Amsterdam, Secretariat, Singel 425, 1012 WP Amsterdam, The Netherlands. You will be contacted as soon as possible.

UvA-DARE is a service provided by the library of the University of Amsterdam (https://dare.uva.nl)

Download date:21 Aug 2022

ChemPubSoc Europe

DOI: 10.1002/cphc.201500195

CHEMPHYSCHEM Reviews

Exploiting Large-Pore Metal–Organic Frameworks for Separations through Entropic Molecular Mechanisms

Ariana Torres-Knoop* and David Dubbeldam*[a]

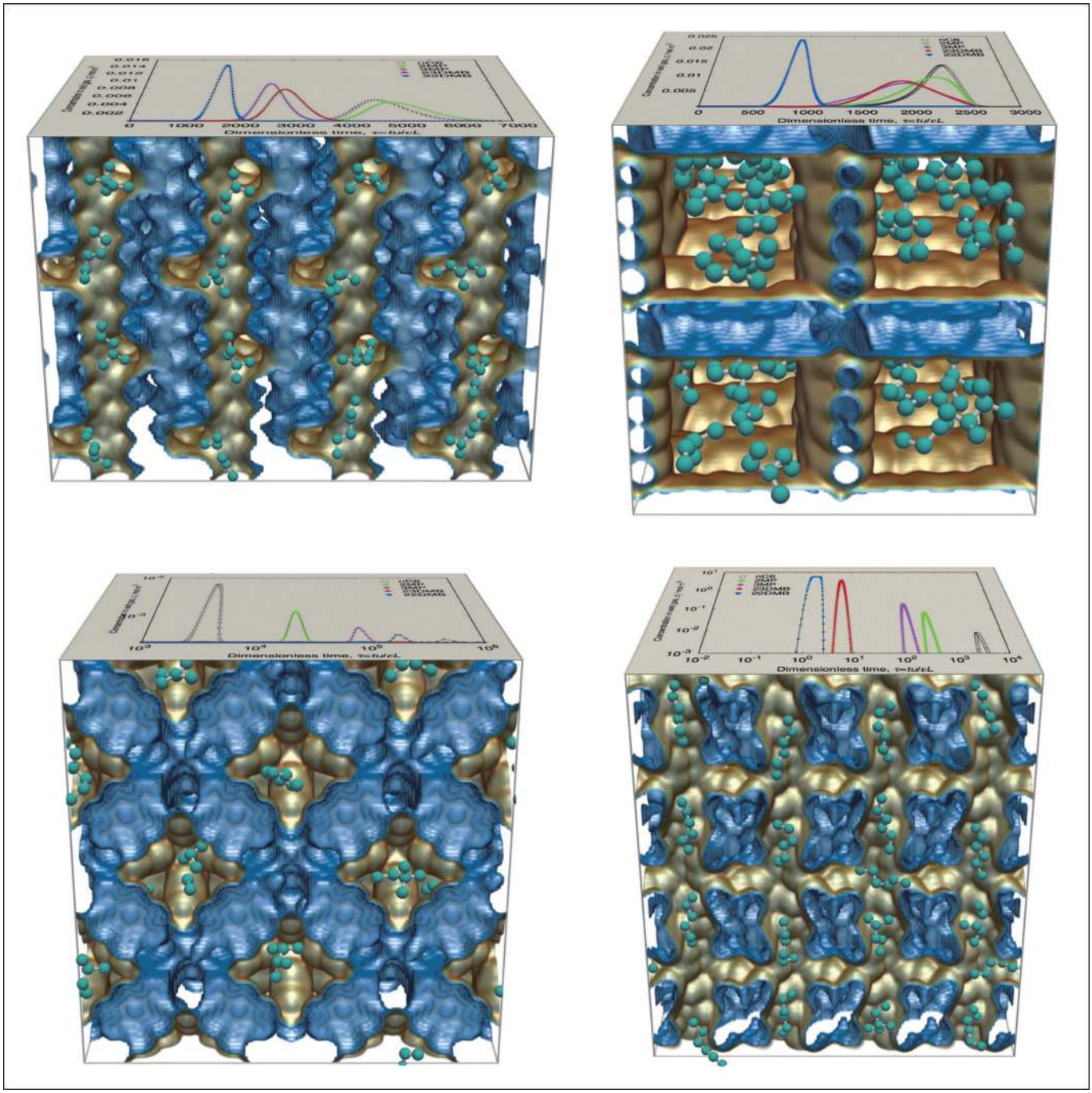

© 2015 Wiley-VCH Verlag GmbH & Co. KGaA, Weinheim

We review the molecular mechanisms behind adsorption and the separations of mixtures in metal–organic frameworks and zeolites. Separation mechanisms can be based on differences in the affinity of the adsorbate with the framework and on entropic effects. To develop next-generation adsorbents, the separation efficiency of the materials needs to be improved. The performance under industrially relevant conditions largely depends on two factors: 1) the separation selectivity and 2) the pore volume capacity of the material. Enthalpic mechanisms can lead to increased selectivities, but these are mostly restricted to the low loading regime, and hence these mechanisms are unable to make use of all of the large-pore volume that a metal–organic framework can provide. Industrial processes routinely operate in the pore saturation regime. In this Review, we focus on entropic molecular separation mechanisms that are effective under these conditions and, in particular, on a recent methodology to obtain high selectivities at high pore loading.

1. Introduction

Nanoporous materials such as zeolites,[1,2] metal–organic frameworks (MOFs),[3–7] and zeolitic imidazolate frameworks (ZIFs)[8] offer great potential as energy-efficient alternatives to conventional separation processes like distillation, absorption, and extraction. Besides being industrially relevant, they are scientifically interesting and allow us to gain an understanding of the fundamentals of the separation mechanisms governing adsorbed molecules in confinement. Separation in nanoporous materials relies on adsorption[9] and diffusion,[10] and can be achieved through size/shape exclusion (steric separation), differences in adsorbate–adsorbent interactions and adsorbate packing (thermodynamic equilibrium effects), as well as differences in the diffusion rate of adsorbates within the adsorbent channels.

Zeolites and aluminosilicates are produced commercially and have relatively high thermal and chemical stabilities. These materials are based on TO_4 tetrahedra (where T is an aluminum or silicon atom), which result in three-dimensional networks when all four corners of the tetrahedron are shared. The tetrahedra are primary building blocks, which form secondary building blocks (e.g. 4-rings, 6-rings, double 6-rings, etc.). These secondary units join together to form the 225 different zeolite topologies we know today. Two well-known zeolites are shown in Figure 1: faujasite (FAU) and Mobile Five (MFI). For FAU, we can see the 6-6, 6-2, 6, 4-2, 1-4-1, and 4 secondary building blocks that form a supercage. The nomenclature can be found in the zeolite atlas, but, for example, 6-6 stands for a double 6-ring of T-atoms. FAU-type zeolites are the most widely used zeolites in catalysis and separation processes. There are many forms of the FAU topology, for example, Ba-X, Na-X, Na-Y, siliceous Na-Y, and SAPO-37, which differ in chemical composition. The FAU-type pore structure consists of sodalite cages arranged in 1.2 nm-wide supercages accessible through 0.72 nm windows. MFI is a typical example of a three-dimensional channel structure with intersections at the crossing of the channels, and has been the focus of pioneering computational zeolite work, starting with the works of June and co-workers.[11–13] The channels of MFI are wide enough to adsorb C6, C7, and C8 isomers, including benzene and xylenes.

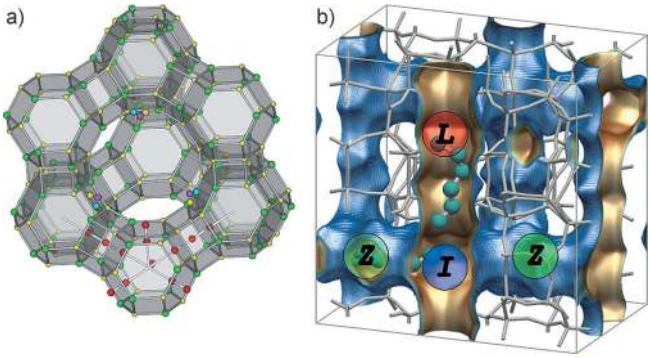

Figure 1. Two well-known zeolites: a) Faujasite (FAU) and b) Mobile Five (MFI). The FAU family of zeolites is composed of sodalite cages linked through double 6-rings into an hexagonal layer. Color code: aluminum (green), silicon (yellow), extra-framework cation site I, I′, II, and II′ (red), site III (blue, pink, yellow). MFI is a three-dimensional network consisting of linear channels (L), zig-zag channels (Z) and intersections (I). The unit cell has dimensions of 20.022×19.889×13.383 Å; there are four intersections, two zig-zag channels, and two linear channels per unit cell. The channels are shown as an adsorption surface (inside as gold, outside view as blue), with hexane molecules adsorbed in the linear and zig-zig channels.

In aluminosilicates, the ratio of aluminum to silicon determines the charge of the framework. This charge is compensated by the presence of extra-framework cations like Na^+, Li^+, K^+, Ba^{2+}, and Ca^{2+}, which are distributed among different sites to maximize interactions with the framework oxygen groups and to minimize cation–cation repulsion. Zeolites have relatively high framework densities, low surface areas, low pore volumes, and, in general, show high selectivities, because strong confinement allows for higher discrimination between adsorbing species.

MOFs are novel materials that, relative to zeolites, have moderate stability, high void volumes, and well-defined tailorable cavities of uniform size. These materials consist of building blocks that self-assemble into crystalline materials that, after evacuation, can find applications in adsorption, separations, air purification, gas storage, chemical sensing, and catalysis.[14–17] MOFs possess almost unlimited structural variety, because of the many combinations of building blocks that can be imagined.[18–20] The clear advantage of MOFs is their incredibly high pore volumes and surface areas. For development of next-generation porous materials, it is highly desirable to combine the high selectivity of zeolites with the large pore capacities of

[a] *A. Torres-Knoop, Dr. D. Dubbeldam*
Van't Hoff Institute for Molecular Sciences, University of Amsterdam
Science Park 904, 1098XH, Amsterdam (The Netherlands)
E-mail: A.TorresKnoop@uva.nl
D.Dubbeldam@uva.nl

© 2015 Wiley-VCH Verlag GmbH & Co. KGaA, Weinheim

MOFs. Another scientifically appealing property of MOFs is their design. Düren et al. developed in silico MOF design, that is, by using information obtained from computer simulation, these authors proposed a new, not yet synthesized, MOF with enhanced methane storage capabilities.[21] Sarkisov and Kim reviewed how the information obtained from computational characterization can be used in screening protocols to identify the most promising materials for a specific application before any costly and time-consuming experimental effort is committed.[22]

There is a conceptual difference between adsorption of small versus large molecules. In contrast to larger molecules, small gas molecules such as CO_2, O_2, N_2, and CH_4 have little or no shape/size differences relative to the framework. They behave more like a fluid inside large pores of nanoporous materials.[23] The possible separation mechanisms are, therefore, limited to either small-pore systems or, in larger pores, limited to reduced separation selectivities. It is inherently difficult for these systems to combine high selectivity with high pore volumes, because only the surface-adsorbed molecules "feel" the framework (whereas the remainder of the molecules interact mainly with other molecules). Selectivity, therefore, originates from the low-loading regime, in which a few molecules interact with strongly selective sites, but selectivity is lost at higher loadings. This is unfortunate, because many industrial processes operate at saturation conditions (e.g. liquid-phase separations).

Separation mechanisms that are effective under saturation conditions must (in general) be entropic in nature (saturation corresponds to the high-pressure part of adsorption isotherms). For molecules that have a bulky size and shape (relative to the framework), it is possible to exploit entropy effects to induce a difference in saturation loading. Molecules that fall into this class include alkanes (chain-like) and aromatics (flat in shape). For example, xylene isomers have the same mass and similar boiling points, and are similar in shape. The similarity of these properties is the reason why they are so difficult to separate through traditional methods. Xylene isomers have a bulkiness that is similar to the shape and size of MOF cavities. If one specific isomer can stack or pack two molecules per channel length, but the other isomers can only stack/pack one, then a significant difference in saturation loading leads to efficient separation. In this case, high selectivity can be combined with high pore volumes. In this Review, we focus on systems of this type and on the methodologies that can be used to achieve them. Our focus lies heavily on computational work because, in simulations, all molecular-level information is readily available and a wide range of thermodynamic conditions can be examined.

Ariana Torres-Knoop received her Bachelor's degree in Physics from the National Autonomous University of Mexico and her Master's degree in Physics and Material Science from a joint program between the University of Amsterdam (Netherlands) and the École Normal Supérieure de Lyon (France). Currently, she is pursuing her Ph.D. program, focusing on exploiting entropic separation mechanisms in nanoporous materials and developing new computational techniques to increase the efficiency and accuracy of the simulations.

David Dubbeldam received his B.Sc. and Ph.D. degree (with honors) from the University of Amsterdam (Netherlands) in Computer Science and Computational Chemistry, respectively. From 2006 until 2009, he carried out a postdoctoral stay at Northwestern University (USA) in the group of Professor Randall Q. Snurr, working on modeling of adsorption and diffusion in flexible MOFs. In 2010, he joined the Computational Chemistry Group at the University of Amsterdam as an Assistant Professor. He is the author of the Monte Carlo and Molecular Dynamics code RASPA aimed at simulations and visualization of adsorption, diffusion, and reactions of adsorbates in nanoporous materials like MOFs, zeolites, and clays.

2. Nanoporous Materials for Separations

Surface area, pore volume, and porosity have become the main characterization properties for bench-marking porous materials.[24] Geometric surface areas can be calculated by using a simple Monte Carlo integration technique, in which a nitrogen probe molecule is rolled along the surface.[21,25] The obtained values usually compare well to Brunauer–Emmett–Teller (BET) surface areas once the appropriate consistency criteria are met.[26] For sorption applications, these molecular surface areas are physically more meaningful than, for example, Connolly surface areas.[27] The crystal volume per mass is a property directly computable from the crystallographic data of a nanoporous material, but it is the accessible volume (the volume accessible to the adsorbates per volume or mass of framework) that is the appropriate adsorption metric. The porosity can be computed by using a methodology proposed by Talu and Myers,[28] in which the volume is probed with a nonadsorbing helium atom. An alternative is to use the $r \rightarrow 0$ limit of the pore-size distribution function to determine the void fraction.[24] Once the helium void fraction and the crystal volume per mass are known, then the accessible pore volume or pore capacity can be calculated (by multiplying the two). The pore capacity is the volume accessible to adsorbates per framework mass, and it takes the framework density and porosity into account. Relevant accessible pore volumes should not include volumes that are not accessible (from the main channel).

Figure 2 shows a plot of surface areas and pore capacities as a function of the porosity of a wide range of MOFs, zeolites, COFs, and ZIFs. Note that the *y* axes are in the log scale. The structures have been selected on the premise that their pores

© 2015 Wiley-VCH Verlag GmbH & Co. KGaA, Weinheim

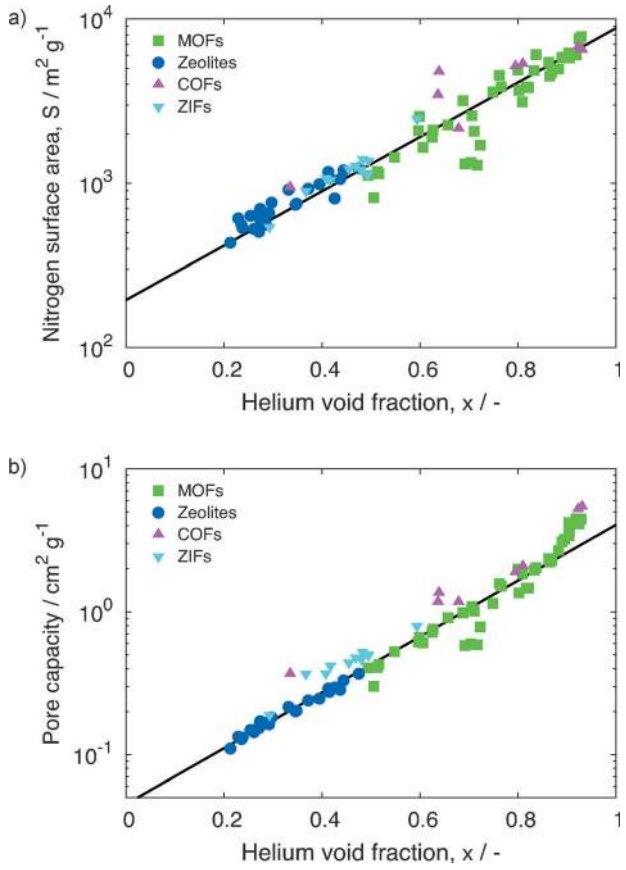

Figure 2. Typical geometric properties of MOFs, COFs, ZIFs, and zeolites. NU-110 has the highest geometric surface area (7400 $m^2 g^{-1}$), whereas COF-108 has the highest pore volume (5.46 $cm^3 g^{-1}$) and void fraction (93.1%). Figure adapted from Ref. [24].

should be large enough to accommodate hexane molecules. In general, the pore capacities and surface areas of MOFs are an order of magnitude larger than those for zeolites. MOFs, therefore, have the potential to revolutionize storage,[29–31] CO_2 capture,[32–34] adsorption,[35] separations,[36] and catalysis,[37–41] to become just as widespread as zeolites.

Figure 3 shows two examples of MOFs: 1) an iron-based MOF with triangular channels and 2) UiO-66 containing cavities accessible through windows. The iron-based MOF has iron-metal corners that are bridged by 4,4-bis(1H-pyrazol-4-yl)biphenyl linkers, creating a one-dimensional, triangular channel structure. The openness of the structure is striking. In contrast to zeolites, which are much denser, every MOF framework atom is in contact with the channel, and the wall thickness is one atomic layer. The channels are large enough to accommodate aromatics without diffusion limitations. The UiO-66 pore system consists of two types of cages per unit cell that alternate, that is, four octahedral cages of 1.1 nm in diameter and eight smaller tetrahedral cages of 0.8 nm in diameter.[42] About 50% of the structure is void. The UiO-66 structure is capable of efficiently separating hexane isomers.[43]

It is also evident (besides noting the high pore volume) that the structures are not as thermally stable as zeolites. MOFs consist of a coordinating metal atom (or cluster of atoms) with one or more ligands attached to it through so-called coordination bonds. These bonds (between 50 and 200 kJ mol^{-1}) are weaker than covalent bonds, and their force acts over a relevant distance of 1.5–2.5 Å. The strength of covalent bonds is about 200–800 kJ mol^{-1} and the force operates over shorter distances on the order of 1–2 Å.[44] In addition, and likely related to this, the structures of MOFs are less water stable than zeolites. The principles of designing water-stable MOFs are not yet well understood. Solvents, left over from the synthesis, need to be removed, usually by heating under vacuum. But, the temperatures that are attainable before thermal decomposition are not as high as those that can be reached for zeolites. There are also issues of (partial) pore collapse and imperfections as well as stacking faults during crystal growth, which can also be seen in zeolites. However, much progress has been made in recent years in the synthesis of (water-)stable MOFs.[45]

There are several works that discuss guidelines and objective criteria, for which the adsorptive delivery should be optimized,[46,47] taking the entire adsorption–desorption cycle into account (in a practical pressure range of 1–30 bar). An affinity of adsorbates for the framework that is too strong makes it energetically costly to desorb, whereas an affinity that is too low leads to poor delivery. For example, for methane, an optimal enthalpy value of around 20 kJ mol^{-1} has been found (at 254 K). Most small-pore structures (like zeolites) have a significantly stronger interaction. MOFs seem to have an ideal ad-

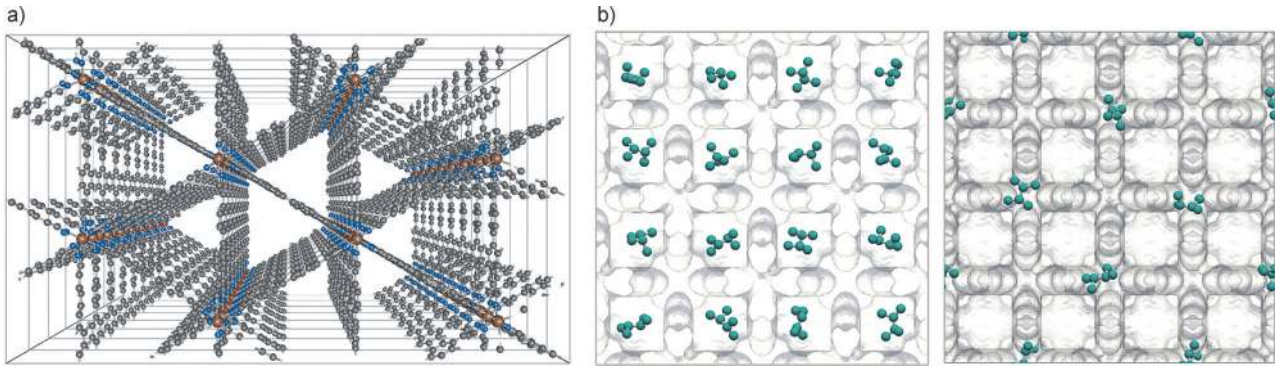

Figure 3. Two examples of MOFs. a) An iron-based MOF with triangular 1D channels running in the *z* direction; the linker molecule is 4,4-bis(1H-pyrazol-4-yl)-biphenyl and the topology of the MOF is the same as $Fe_2(BDP)_3$, but has an additional phenyl group in the linker, and the channels are large enough to accommodate aromatics. b) UiO-66 consisting of two types of cages in an alternating arrangement: left) small cavities and right) large type cavities. We show a snapshot of 2,3-dimethylbutane at high loading at 433 K in 2×2×2 unit cells. Each edge length of the unit cell is 20.7 Å.

© 2015 Wiley-VCH Verlag GmbH & Co. KGaA, Weinheim

sorption behavior for many adsorbates, except perhaps for hydrogen adsorption (MOFs are still well below the Department of Energy targets for hydrogen storage, although progress has been made).[48] For example, the record holder for methane storage is a MOF.[49] However, because the building blocks of MOFs are expensive, it would be costly to use MOFs for storage applications. For separation and catalysis applications, the material can be immediately reused and the cost of the material itself is less of an issue (especially if the MOFs are stable). The open structure of MOFs means that there are little or no diffusion limitations.[50] A wish list for a next-generation adsorbents would therefore include:

- sufficient thermal and water stability
- high adsorption selectivity
- large pore capacity
- heats of adsorption that are not too low or too high
- a diffusion selectivity that enhances the adsorption selectivity even further (or at least does not hamper the adsorption selectivity).

Operating under saturation conditions and using large pore capacities are benificial, because more fluid can then be treated in a single adsorption–desorption cycle, thereby reducing the number of cycles (and hence the costly desorption step). For membrane applications, in particular, it is the product of both the diffusivity and adsorption selectivities that determines the efficiency. This is inherently difficult, because usually (but fortunately not always) an increase in affinity decreases the diffusion rate.

3. Adsorption Thermodynamics

The thermodynamics of physisorption of gases in porous solids is well developed (see Refs. [51–53] and references therein). Excess adsorption is defined as "the difference between the number of moles of gas present in the system (a sample cell containing a porous solid) and the number of moles that would be present if all of the accessible volume in the system (both inside and outside the pores) was occupied by the adsorbate gas in its bulk state at the same temperature and pressure".[54] Although experiments measure excess adsorption, it is much more convenient (and necessary) to describe the theoretical framework in terms of absolute adsorption.[54] Simulations always compute absolute adsorption n_a, but (knowing the accessible pore volume V_{pore} of the framework) n_a can be converted to excess adsorption n_{exc} by using Equation (1):

$$n_{exc} = n_a - \frac{pV_{pore}}{zRT} = n_a - \rho(p,T)V_{pore} \quad (1)$$

in which $R = 8.31451\ \mathrm{J\,mol^{-1}\,K^{-1}}$ is the gas constant, z is the compressibility in the bulk fluid phase, and ρ is the density of the bulk fluid phase at temperature T and pressure p.

The affinity of a molecule to the framework can be expressed as the binding energy, or more generally, as the enthalpy of adsorption at infinite dilution ΔH [Eq. (2)]:[55]

$$\Delta H = \Delta U - RT = \langle U_{hg}\rangle - \langle U_h\rangle - \langle U_g\rangle - RT \quad (2)$$

where ΔU is the internal energy, and $\langle U_{hg}\rangle$, $\langle U_h\rangle$, and $\langle U_g\rangle$ are the average energy of the guest molecule inside the host framework, the average energy of the host framework, and the average energy of the guest molecule, respectively. In simulations, a common approximation is to assume the framework is rigid and, in this case, the enthalpy of adsorption at infinite dilution can be understood to be the difference in internal energy of a single molecule outside and inside the confinement of the host framework. At the limit of zero temperature, the enthalpy of adsorption becomes the binding energy. The infinite dilution enthalpy of adsorption ΔH is related to Henry's coefficient K_H through Equation (3):

$$\Delta H = -\frac{\partial lnK_H}{\partial \beta} \quad (3)$$

where $\beta = 1/(k_B T)$ is the inverse temperature and k_B the Boltzmann's constant. Henry's coefficient is the slope of the isotherm at zero pressure/loading.

The Helmholtz free energy ΔA of adsorption can be computed by using the Widom test-particle insertion. At infinite dilution, the Gibbs free energy ΔG is related to the Helmholtz free energy ΔA through Equation (4):

$$\Delta G = \Delta A - RT \quad (4)$$

The entropy difference ΔS between a molecule outside and inside the framework is given as Equation (5):

$$\Delta S = \frac{\Delta U - \Delta A}{T} = \frac{\Delta H - \Delta G}{T} \quad (5)$$

The Gibbs free energy of adsorption consists of a change in enthalpy ΔH and a (temperature) change in entropy $T\Delta S$:

$$\Delta G = \Delta H - T\Delta S \quad (6)$$

So, when a molecule adsorbs, it transitions from the free fluid phase to an adsorbed phase with two common contributions:

1. It (usually) gains favorable energy (ΔH is negative), because of attractive interactions with the framework.
2. The molecule has an increased confinement compared to the gas phase, thereby loosing entropy (ΔS is negative, $-T\Delta S$ is positive, leading to increased and less favorable ΔG).

Adsorption will only occur when ΔG is negative, and this is only possible if $\Delta H < T\Delta S$. The process is (usually) exothermic ($\Delta H < 0$). Figure 4 plots ΔG, ΔH, and $-T\Delta S$ as a function of pore size at 533 K. The data is taken from the report by Schenk et al.[56] For hexane, the adsorption strength ΔG is stronger in the tighter MTW channels, even though the hexane molecule

© 2015 Wiley-VCH Verlag GmbH & Co. KGaA, Weinheim

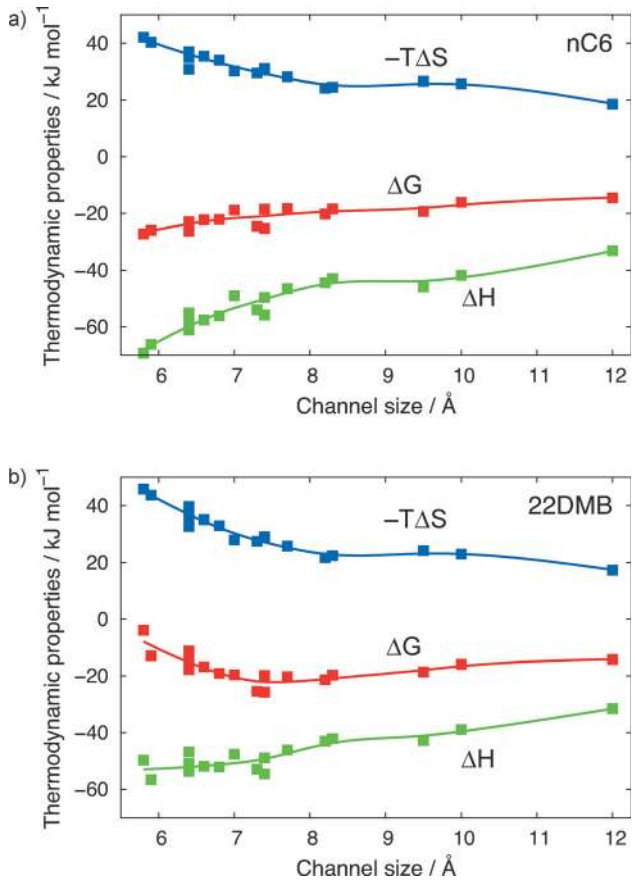

Figure 4. Thermodynamic adsorption properties of a) hexane (*n*C6) and b) 2,2-dimethylbutane (22DMB) as a function of channel size. The zeolites are in order of smallest to largest: MTW, VET, SPE, BEA, SSZ-31, MOR, CON, OFF, GME, AFI, CFI, MAZ, ADR, DON, AET, MEI, LTL, and FAU. Lines are guides to the eye. Data taken from Ref. [56].

is more confined, as this is offset by a larger enthalpy gain with the structure. For hexane, ΔG nicely correlates with the channel diameter, but, for 2,2-dimethylbutane, there is an optimal channel width somewhere in between FAU and MTW (i.e. AFI with pore size of 7.3 Å).[56,57] In general, the interplay of enthalpy and entropy is difficult to predict.

As another example, we show the values of ΔH, ΔG, and $-T\Delta S$ for hexane isomers in UiO-66 in Table 1. At low loading, the hexane isomers prefer the small cages in UiO-66, whereas at high loading the isomers also occupy the larger cages. The branched hexane isomers are preferred in these small cages over mono-branched and linear hexane. At 300 K, 2,3-dimethylbutane is preferred, whereas at higher temperatures 2,2-dimethylbutane is preferred. This is exclusively attributed to entropy. In structures like UiO-66, the molecules are well separated in small cavities, and intermolecular interactions for hexane isomers are low. In general, because there are two types of cavities in UiO-66, molecules of a certain type can preferentially adsorb in one of the two types of cage (or transition between them), depending on the temperature and loading.[58] Entropy differences between components in a mixture can be substantial, even at low loading, and mixture separations can be driven by rotational entropy.[43,59]

Table 1. Thermodynamic adsorption properties of hexane isomers at infinite dilution in UiO-66 at 300, 400, and 500 K. The structure of UiO-66 is shown in Figure 3.

T [K]	Adsorbate	ΔG [kJ mol^{-1}]	ΔH [kJ mol^{-1}]	$-T\Delta S$ [kJ mol^{-1}]	ΔS [J mol^{-1}]
300	22DMB	−50.6	−71.9	21.3	−70.8
300	23DMB	−55.7	−77.5	21.8	−72.8
300	2MP	−44.8	−70.4	25.6	−85.3
300	3MP	−48.8	−72.8	24.0	−80.2
300	*n*C6	−37.2	−64.0	26.8	−89.2
400	22DMB	−56.0	−71.5	15.5	−38.9
400	23DMB	−46.1	−77.3	31.2	−78.0
400	2MP	−35.3	−69.1	33.7	−84.3
400	3MP	−42.3	−71.8	29.4	−73.6
400	*n*C6	−23.0	−62.8	39.8	−99.4
500	22DMB	−51.3	−71.3	20.0	−40.0
500	23DMB	−39.8	−77.0	37.2	−74.4
500	2MP	−28.1	−67.8	39.7	−79.4
500	3MP	−36.0	−71.0	35.0	−70.0
500	*n*C6	−15.3	−61.4	46.0	−92.0

At the start of an adsorption process, $\Delta H < T\Delta S$ and $\Delta G < 0$, and the process transfers molecules in the direction of lower free energy (which results in adsorption). As the adsorption process continues, the ΔH and $T\Delta S$ terms change until $\Delta H = T\Delta S$ and $\Delta G = 0$, and equilibrium is achieved. At finite loading, the enthalpy of adsorption ΔH can be computed in the grand-canonical ensemble μVT (with fixed chemical potential μ, fixed volume V, and fixed temperature T) from a fluctuation formula given by Equation (7):[60,61]

$$\Delta H = \frac{\langle U \times N\rangle_\mu - \langle U\rangle_\mu \langle N\rangle_\mu}{\langle N^2\rangle_\mu - \langle N\rangle_\mu^2} - \langle U_g\rangle - RT \tag{7}$$

The chemical potential in the adsorbed μ_a and gas phase μ_g are defined by Equations (8) and (9), respectively:

$$\mu_a = \left(\frac{\partial G_a}{\partial n_a}\right)_{T,p} \tag{8}$$

$$\mu_g = \left(\frac{\partial G_g}{\partial n_g}\right)_{T,p} \tag{9}$$

When equilibrium is reached, the chemical potential of the adsorbed phase becomes equal to the gas-phase chemical potential [Eq. (10)]:

$$\Delta G = (\mu_a - \mu_g)\, dn_a = 0 \rightarrow \mu_a = \mu_g \tag{10}$$

Adsorption is usually described through isotherms, that is, the amount of adsorbate on the adsorbent at constant temperature as a function of pressure or fugacity. A common, generic isotherm model is the *n*-site Langmuir–Freundlich (LF) model (also known as the Sips model) [Eq. (11)]:

$$q(x) = \sum_i^n q_{i,\mathrm{sat}} \frac{b_i x^{\nu_i}}{1 + b_i x^{\nu_i}} \tag{11}$$

© 2015 Wiley-VCH Verlag GmbH & Co. KGaA, Weinheim

where x can be pressure or fugacity, n is the number of types of sites, and $q_{i,sat}$ (the saturation loading for site i), b_i, and v_i are fitting constants. The constant v is often interpreted as the heterogeneity factor.[62] Values of unity indicate a material with homogeneous binding sites and Equation (11) reduces to the n-site Langmuir model.

Our knowledge of the peculiarities of isotherm behavior has grown tremendously during the last two decades. Hexane and heptane in MFI show inflections in the isotherms, owing to commensurate freezing.[63] The length of these molecules is commensurate with the length of the zig-zag channels. In Figures 5 a and 5 b, we show the density of hexane atoms in the MFI structure. The images can be considered an average over millions of snapshots. Hexane fits snugly and packs nicely in the zig-zag channels without sticking out into the intersections. Only the hexane molecules that are in the linear channels can stick out into the intersection.

By fitting the isotherms to a model and by examining simulation snapshots of the system, a lot of information can be obtained.[24] Branched alkanes in MFI can be described by the dual-site Langmuir model,[64] which signals the absence of significant intermolecular interactions. In Figure 5 c, we show the adsorption isotherms of linear alkanes[65] and their dual-site LF fits (Table 2). The model describes the isotherms well. Linear alkanes that are smaller than hexane have a lot of rotational freedom (i.e. several molecules can fit in the channels and intersections) and there is much heterogeneity. For small molecules, the intersections are comparatively unfavorable, owing to a high potential energy and low entropy.[66] Adsorptions in the straight and zig-zag channels have very similar potential energies, but the zig-zag channel is slightly more favored, owing to its higher entropy.[66,67] Hexane is most commensurate with the zig-zag channel and represents the onset of the behavior for longer alkanes, all of which have large inflections. They are no longer hidden inside the zig-zag channels, and when there are more than four molecules per unit cell, they must interact with each other. The magnitude of the inflection increases for lower temperatures (which signals an energetic origin),

Table 2. Dual-site Langmuir–Freundlich parameters for pure-component linear alkanes at 303 K in MFI.

Alkane	Site A			Site B		
	$q_{i,A,sat}$ [molec. uc^{-1}]	$b_{i,A}$ [Pa$^{-\nu_{i,A}}$]	$\nu_{i,A}$ [-]	$q_{i,B,sat}$ [molec. uc^{-1}]	$b_{i,B}$ [Pa$^{-\nu_{i,B}}$]	$\nu_{i,B}$ [-]
*n*C4	7.83	2.08×10^{-3}	1.34	2.35	2.20×10^{-2}	0.42
*n*C5	7.56	1.01×10^{-1}	1.30	1.28	1.06×10^{-1}	0.27
*n*C6	7.57	1.34×10^{0}	0.86	0.43	9.04×10^{-4}	1.42
*n*C7	4.02	1.55×10^{2}	1.15	2.97	8.20×10^{-3}	1.38
*n*C8	3.97	4.73×10^{3}	1.16	2.02	5.50×10^{-3}	0.64
*n*C9	4.00	5.92×10^{4}	1.10	1.00	3.25×10^{-2}	0.96

In hindsight, almost all isotherms in nanoporous materials have inflections. The underlying cause of inflections is an energetic and entropic difference between sites in the structure. If the sites differ greatly in the energetics, the lowest energy site is first filled before the next site is (e.g. branched alkanes in MFI), and this second filling requires significantly more pressure. For smaller energy differences, the adsorption occurs concurrently, but is mostly in favor of the lowest energy site. The magnitude of an inflection is so strongly related and so sensitive to the energy difference between the sites that accurate force field parameters can be obtained by fitting molecular models to adsorption isotherms with inflections.[68] Also, large-pore MOFs show inflections, even for small molecules. Walton et al. showed that the pressure of the pore filling shifts toward the bulk condensation pressure with increasing pore size (IRMOFs-1, -10, and -16).[23] This means that the original fluid behavior is largely retained for small adsorbates in large-pore MOFs, and inflections of this type are attributed to effects that are already present in the fluid phase.

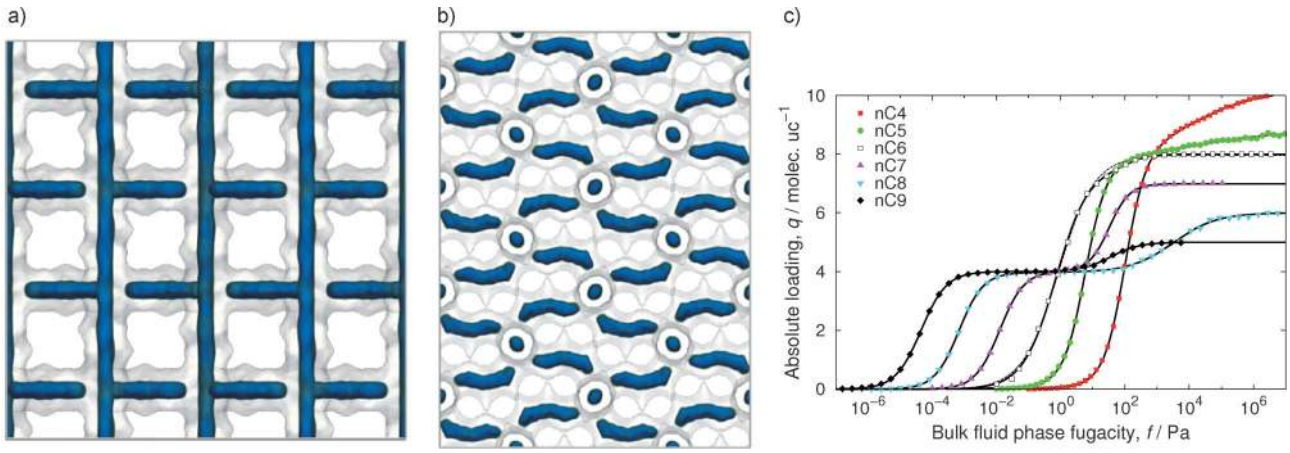

Figure 5. Commensurate freezing of hexane and heptane in MFI: a) front view of the density of hexane atoms in MFI, b) top view of the density of hexane atoms in MFI, and c) single-component isotherms of linear alkanes in MFI at 303 K. The solid lines are dual Langmuir–Freundlich fits through the isotherm data. For hexane, a dashed line shows the fit of a single Langmuir–Freundlich fit (there is a small difference at 7.5 molecules per unit cell). The simulations were run long enough to make sure the error bar was smaller than the symbol size.[65]

© 2015 Wiley-VCH Verlag GmbH & Co. KGaA, Weinheim

4. Enthalpic Separation Mechanisms

Most studies aim to improve the separation (and storage) efficiency of materials focusing on tuning the enthalpy of adsorption, because it is much harder to elucidate the entropy contribution as a function of topology. The entropy effects can (in general) only be studied by doing explicit simulations, and represent one of the reasons for performing screening studies, in which a large dataset of structures is examined for adsorption performance. The tuning of the heat of adsorption involves changing the affinity of an adsorbate with an adsorption site, which is easier to reason and think in terms of design rules. For storage, the affinity should be relatively high, but not too high or the adsorbate component will be difficult to desorb. For mixture separations, there should be (in addition to lying in a limited range of enthalpies of adsorption) also be a large difference in affinity between the components. Before turning to the entropic effects, which is the main focus, we briefly review some examples of how the affinities of adsorbates to the framework might be adjusted. Simulation works have been crucial for a better understanding since the origin of adsorption can be studied in high detail and the magnitude of effects can be studied by breaking down the total adsorption affinity into its indivudual components (such as vdW, polarization, charge-transfer effects, etc). We will only discuss a few physisorption examples and focus on two well known applications: hydrogen storage and CO_2 separation from flue gases mixtures.

Hydrogen storage is recognized as one of the critical steps towards using hydrogen as an alternative energy resource. For storage applications, the affinity of the adsorbate with the adsorbent has to be sufficiently high. Computational studies[69–71] showed that doped materials store more hydrogen molecules under the same conditions than nondoped ones, owing to the strong interaction between the hydrogen quadrupole moment and the charged ions. Fischer et al.[72] studied the influence of substituents on the strength of the copper–hydrogen interaction and showed that electron-withdrawing substituents, such as nitro or cyano groups, lead to a signficant increase of the interaction energy, whereas electron-donating substituents weaken the interaction. An analysis of the DFT electron density revealed a correlation of the interaction strength with the Hirshfeld charge at the Cu site, showing that the increase in interaction energy is directly related to the increased positive polarization of the metal site. Kuc et al.[73] showed that the adsorption mechanism of H_2 in IRMOF-1 is governed by weak London dispersion. Polarizability has a negligible contribution, as the charge distribution in the MOF is not large enough to create a dipole moment in the metal–oxygen bond.

Separation of CO_2 from the rest of the natural gas mixture is critical for environmental protection and sustainable development. CO_2 separation through adsorption can be achieved by exploiting the larger dipole moment and polarizability of CO_2 compared to other natural gas mixture components like N_2, H_2, O_2, CO, and CH_4. Selective adsorption of CO_2, owing to its strong interaction with unsaturated metal sites, has been observed experimentally in Cu-BTC,[74,75] Cu-TDPAT,[76] and M-MOF-74.[77–82] A simulation study by Yang et al.[83] showed that the selectivity of CO_2 from flue gas mixtures in Cu-BTC arises from the difference in quadrupole moments. Introducing ions into MOF systems generally leads to enhanced adsorption and selectivity for CO_2, which is the case in Na-X zeolite[84] and rho-ZMOF.[85] Other examples include simulation studies by Barbarao and Jiang[86] in a Na-cation-loaded MOF with rho-topology, and by Jiang[87] who studied soc-MOF with extra framework NO_3^- ions. CO_2 selectivity can also be enhanced by substituting functional groups ($-NH_2$, $-OH$, CH_3, Cl, F, Br, CN) in the MOF linkers.[88–90] Yang et al. computationally studied the effect of adding charge-withdrawal functional groups [C_6H_6, chlorine group (C_6H_5Cl), and nitro group (C_6H_5N)] to ZIF-68, ZIF-69, and ZIF-78.[91] These authors showed that the withdrawal of electronic charge from the linker leads to enhanced acidity for the hydrogen atoms on the linker, which can form weak hydrogen-bond interactions with the oxygen atoms of CO_2. They also found that the binding capacity of the linker with a nitro functional group for CO_2 is much higher, owing to the strong effect of the nitro group on polarizing the CO_2 molecule. Torrisi et al.[92] studied the effect of introducing polar groups (NO_2, NH_2, OH, SO_3H, and COOH) into benzene linkers. They showed that the strongest interaction is with the lone-pair-donation atoms (N, O) of the side groups. The CO_2 molecule can be polarized by this lone-pair interaction and by the hydrogen-bonding interaction. Yazaydin et al.[93] showed that the CO_2 uptake and its selectivity over N_2 and CH_4 in Cu–BTC are significantly increased in the presence of water. These molecules coordinate to the open-metal sites in the framework and create an additional electric field that strongly interacts with the CO_2 quadrupole moment. Zhang and co-workers have given a good Review on CO_2 separations.[94] Burtch et al. showed that the number of nonpolar functional groups on the benzene dicarboxylate linker in the pillared DMOF structure is an effective way to tune the CO_2 Henry's coefficient in this isostructural series.[95] Park et al. tuned the binding affinity of CO_2 for M-MOF-74 through metal substitution (M = Mg, Ca, and the first transition-metal elements) and showed that Ti- and V-MOF-74 can have enhanced affinities compared to Mg-MOF-74 by 6-9 kJ mol^{-1}.[96] MOF-74 is an interesting system, because CO_2 molecules become polarized near metal atoms, which results in a stronger interaction than could be accounted for in a fixed-charge model.[97,98]

Other interesting studies exploiting enthalpic effects for separation include the use of differences in the quadrupole moments of N_2 and O_2 to favor N_2 adsorption in various structures like LTA-4A and LTA-5A,[99,100] and Cu-BTC.[101] Also, differences in the magnetic susceptibilities can be exploited to enhance the affinity of O_2 over N_2 in MOF-177.[102] Selective adsorption of $CHCl_3$, MeOH, and H_2O over hexane or pentane in Zn_2(bptc)[103] and of C_2H_2 over CO_2 in Cu_2(pzdc)$_2$(pyz)[104] has been found to be caused by hydrogen bonding with the oxygen atoms, whereas the separation of alkane/alkene mixtures are achieved through π-interactions between the metals and the double bonds of alkenes. For example, Wang et al.[74] observed selectivity of ethylene over ethane in Cu–BTC, Yoon et al.[105] and Lamia et al.[106] observed selectivity of propylene

© 2015 Wiley-VCH Verlag GmbH & Co. KGaA, Weinheim

over propane in Cu–BTC, and Hartmann et al.[107] found selectivity of isobutene and isobutene in Cu–BTC.

MOFs differ from zeolites in that they can possess unsaturated (open) metal sites. These sites can be strong and selective, and have opened up a promising future for MOFs as catalysts. Zeolites, on the other hand, can possess strong electric-field gradients when cations are incorporated. Zeolites that are used in industry usually contain cations, for example, Na-X, Ba-X, Na-Y, LTA-4A (sodium ions) and LTA-5A (sodium and calcium ions). Introducing cations into MOFs can lead to increased an affinity for certain adsorbates. For example, several studies have used lithium doping as a method to increase the affinity of hydrogen to the MOF[108–110] to provide the desired binding enthalpies in the range of 20–30 kJ mol^{-1} for hydrogen. Mulfort and Hupp[109] reasoned that framework reduction might increase the affinity by: 1) increasing the polarizability of organic struts, thereby strengthening adsorbate/framework van der Waals interactions; 2) introducing charge-compensating cations capable of binding gas molecules through charge/quadrupole or more specific interactions; and 3) coulombically displacing interwoven frameworks, thereby enhancing accessible surface area.

5. Entropic Separation Mechanisms

5.1. Entropy

In a mixture, one component can drive another out at high pressures. Differences in adsorption loading of a mixture can be caused by energetic differences in the affinity of the components and by entropic effects. There are several tests to get to the root-cause of the expulsion effect:

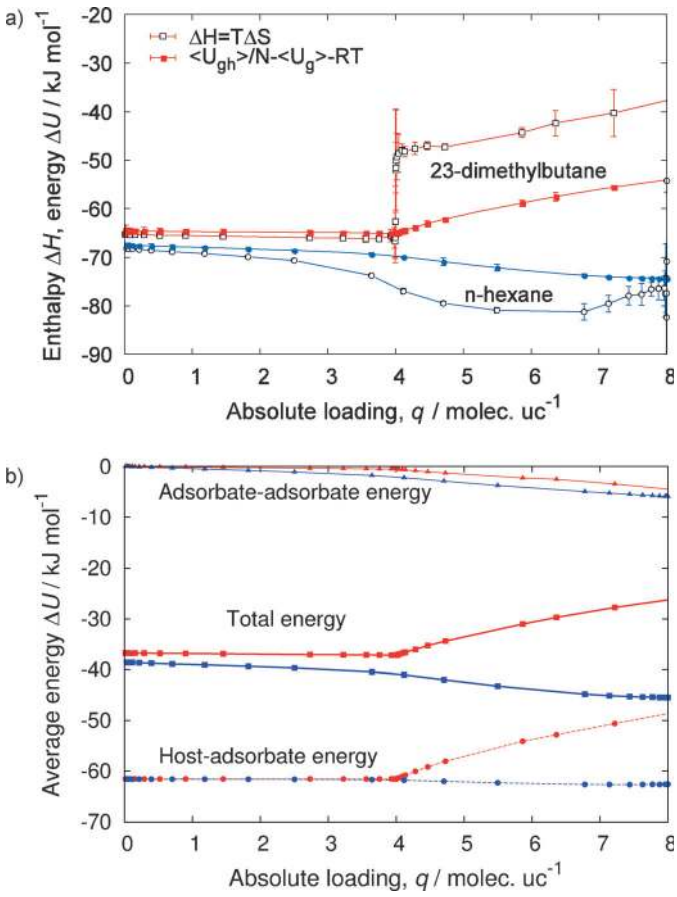

Figure 6. Elucidating enthalpy versus entropy: a) enthalpy of adsorption and average energy in MFI at 433 K for hexane and 2,3-dimethylbutane; b) average energies of the adsorbed phase (total, adsorbate-host, and adsorbate-adsorbate energy [intra-molecular energy not shown]).

- **Examine the heat of adsorption and compare to the average energy** (as a function of loading). Each point of the isotherm is at equilibrium and, hence, $\Delta H = T\Delta S$. At infinite dilution, the enthalpy is directly related to the difference in internal energy [see Eq. (2)]. So, when we plot ΔH as a function of loading (at constant temperature), any sudden changes signal sudden changes in entropy. When compared to the average energy $\langle U_{hg}\rangle/N - \langle U_g\rangle - RT$ (which does not contain entropy), the effects of enthalpy and entropy can be elucidated. For example, in Figure 6, we plot the enthalpy of adsorption as a function of loading for hexane and 2,3-dimethylbutane in MFI. For hexane, energetics and entropy go hand-in-hand; the hexane molecules at loadings higher than four molecules per unit cell have significant favorable intermolecular interactions, which increasingly confine the molecules. The di-branched molecules adsorb in the intersections of MFI first (see Figure 1 b for the structure of MFI) and, as soon as these are filled (four molecules per unit cell), the di-branched molecules are pushed into the linear and zig-zag channels, thereby creating an additional adsorption lattice that was not energetically favorable before. Doubling the amount of available sites causes a sudden jump in the entropy. The creation takes a large additional driving force (as the channel sites are energetically unfavorable for the branched isomers), leading to large inflections in the isotherms. We will discuss this further in Section 5.4. Note the large scatter in ΔH at high loading. The fluctuation method relies on the efficiency of insertion and deletions of the particle during the simulation and, therefore, generally fails close to saturation loadings.
- **Change the interaction model of the atoms to a hard-sphere model.**[11] If the attractive part of the Lennard–Jones potential is removed from the framework–adsorbate and adsorbate–adsorbate interactions, and the repulsion term is extremely strong, then the atoms are treated as impenetrable spheres that cannot overlap in space. Such a hard-sphere model has no energy scale and the only driving force is entropy. If, in a mixture, one of the components is driven out at high pressures, then this must be because of entropy.
- **Investigate the effect as a function of temperature.** The lower the temperature, the more energetics dominates. Vice versa, entropy becomes increasingly important at high temperatures. In Figure 7, we show the component loading in a C2, C4, C6 equimolar mixture in a TON-type zeolite with a constant total loading. As can be observed, with an increase in temperature, and hence $T\Delta S$, the smallest com-

© 2015 Wiley-VCH Verlag GmbH & Co. KGaA, Weinheim

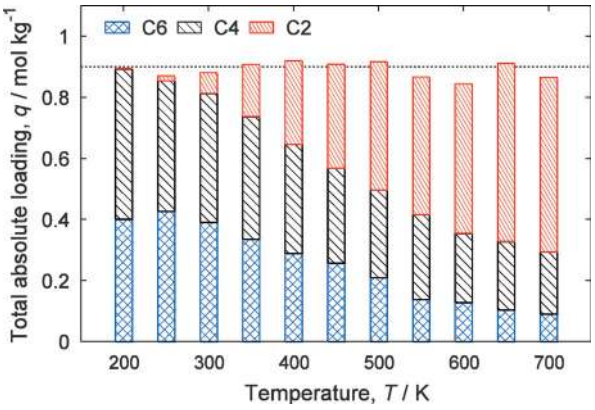

Figure 7. Elucidating enthalpy versus entropy: component loading of an equimolar C2, C4, C6 mixture in a TON-type zeolite at an (approximately) fixed total loading of 0.9 mol kg^{-1} (dashed line) as a function of temperature.

ponent will win (this will be further discussed in Sections 5.2 and 5.3).

Molecules may be separated by selective adsorption on the basis of differences in their molecular shape.[112] Krishna et al. reviewed entropy effects on the adsorption of mixtures of alkanes[113] and packing effects in microporous materials.[114] Smit and Maesen reviewed adsorption and shape selectivity in zeolites.[115,116]

For alkanes, three entropy effects were discovered: 1) size entropy,[117] 2) length entropy,[117] and 3) configurational entropy.[64,111,118] The prominent geometric property that characterizes linear alkanes is the chain length. Branched alkanes, compared to linear isomers, exhibit a decreased length, but also an increased width. Recently, two new entropic effects were found for the adsorption of a mixture of aromatics. The typical characteristic of aromatics is their relatively small height compared to their width and length (i.e. the aromatic ring is flat). We will first discuss the closely related size and length entropy effects. Then, we will discuss configurational entropy, afterwards we will discuss two more recently discovered entropic mechanisms, that is, commensurate stacking and face-to-face stacking (i.e. pringling).

5.2. Size Entropy

Size entropy favors smaller molecules over larger molecules.[117,119] At low loadings, the larger molecules adsorb most strongly (highest adsorption strength and Henry coefficients). However, because the smaller molecules can fill the vacant sites more easily, their saturation loading is usually significantly higher than for longer molecules, in terms of molecules per unit cell. The entropy gain is so strong that replacing one C6 by two C2 units is favorable, even though the number of carbon atoms becomes lower (so it is misleading to think of entropy in terms of, for example, the total amount of carbon atoms). The higher saturation capacity of the smaller molecules increases the entropy of the system (and reduces the Gibbs free energy), favoring the adsorption of smaller molecules over

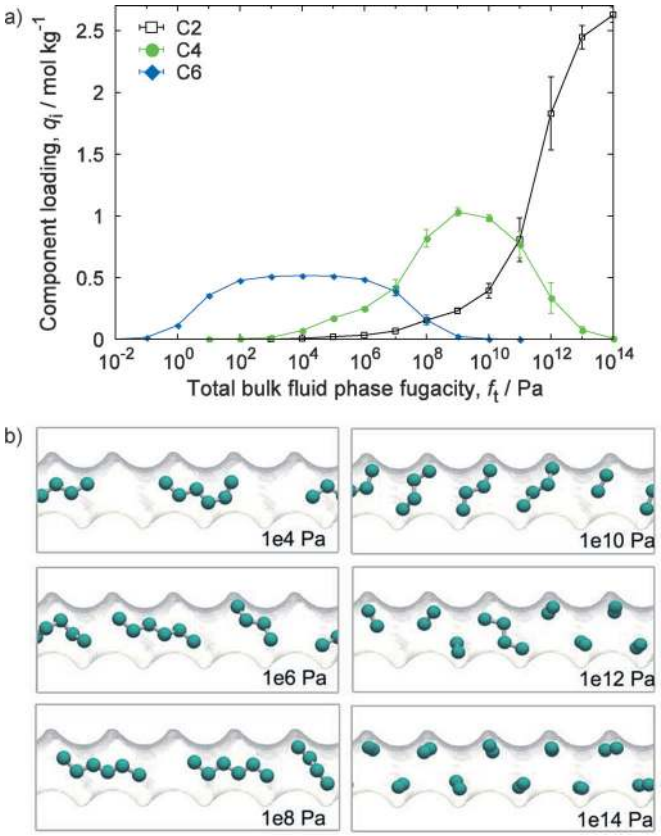

Figure 8. Size entropy in TON: a) isotherms for an equimolar mixture of C2, C4, C6 in TON zeolite at 300 K; b) snapshots of a three-components equimolar mixture of C2, C4, C6 linear alkanes at 300 K in TON.

larger molecules under saturation conditions. This has been observed for alkane mixtures that differ in chain length (and hence in molecular volume) in MFI under saturation conditions.[120–122] In all cases, the more bulky component adsorbs the strongest at low loading, but is eventually overtaken by the smallest component.

In Figure 8, we show this behavior for an equimolar C2, C4, C6 mixture of linear alkanes in a TON-type zeolite. The TON-type zeolite is a one-dimensional channel zeolite consisting of apertures of 8-rings of about 5.7 Å in diameter. At low loadings, C6 has the strongest affinity (heat of adsorption at infinite dilution and 300 K are C2 = −31 kJ mol^{-1}, C4 = −54 kJ mol^{-1}, and C6 = −77 kJ mol^{-1}) and highest Henry coefficient, because it has more carbon atoms. However, as the fugacity increases, C6 molecules are replaced by C4 molecules and, afterwards, by C2 molecules. This is because, under saturation conditions, the dimensions of TON channels restrict the adsorption of C6 to two molecules per unit cell, of C4 to five molecules per unit cell, and of C2 to ten molecules per unit cell (as shown in Figure 8 b), which increases the overall entropy of the system. The size entropy effect counters the energetic effect of the larger number of carbon atoms, which favors the adsorption of the larger molecule, and the adsorption of C6 in TON is eventually overtaken at higher fugacities by the smallest component, C2.

In Figure 7, the loading of C2, C4, and C6 at a total mixture loading of 1.5 molecules per unit cell is presented as a function

© 2015 Wiley-VCH Verlag GmbH & Co. KGaA, Weinheim

of temperature. We can see that, at low temperatures, TON is C6 selective, but with increasing temperature the system becomes more C2 selective. This means that C2 is entropically favored over C4 and C6, whereas C4 is favored over C6. If the temperature increases, the entropic effects become dominant over the enthalpic effects.

The size entropy separation mechanism requires a difference in the molecular volume of the components. For example, when we examine the same equimolar C2, C4, C6 mixture of linear alkanes in a FAU-type zeolite (which has a large, roughly spherical cavity), we observe the same behavior, that is, the smallest C2 molecule wins at high pressures. It does not depend on the topology of the framework, but on the differences in saturation loading. In Table 3, we list geometric properties of hexane isomers, and we show the pure component adsorption of hexane isomers in FAU-type zeolite in Figure 9. As can be seen, because the hexane isomers have similar molecular surface areas and volumes (with the exception of 2,2-dimethylbutane), size entropy is of no use here. For this, we need to turn to length entropy, which makes use of differences in the length direction of the isomers(L_x in Table 3).

Table 3. Molecular properties of hexane isomers: surface area (vdW), volume (vdW), and shadow lengths[123] calculated using Materials Studio[124] by projecting the molecular surface on three mutually perpendicular planes. The molecules are first rotated to align the principal moments of inertia with the *x*, *y*, and *z* axes.

Adsorbate	Surface area [Å^2]	Volume [Å^3]	L_x [Å]	L_y [Å]	L_z [Å]
23DMB	116.35	86.81	6.71	6.21	4.04
22DMB	111.71	84.16	7.11	5.71	5.44
3MP	114.83	86.10	7.83	6.00	3.43
2MP	116.14	85.4	8.24	5.87	3.98
*n*C6	116.28	85.26	9.85	4.42	3.64

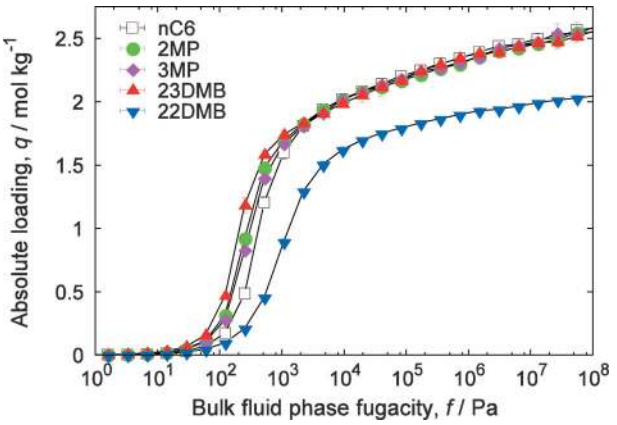

Figure 9. Single-component isotherms of C6 isomers at 300 K in FAU.

5.3. Length Entropy

Although size entropy cannot separate a mixture of hexane isomers in a large-pore structure like FAU (the different hexane isomers have more or less the same volume; see Table 3), it is possible to modify the effective size of a molecule. For example, by lining up the hexane isomers in one-dimensional channels, the dominant effective size that comes into play is its length (Table 3 shows that the length L_x of the hexane isomers are significantly different). The length entropy concept is depicted schematically in Figure 10. Basically, in one-dimensional channels, size is best described in terms of length. Length entropy has been highlighted by Talbot[117] and the term is derived from the decreasing linear dimension of the molecule.[125]

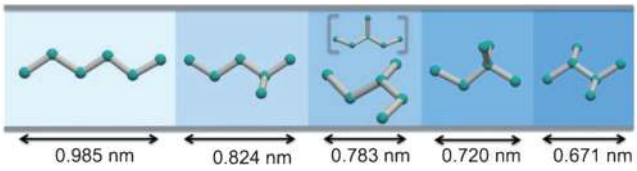

Figure 10. Length entropy of C6 isomers in one-dimensional channels. The projected length are *n*C6 > 2MP > 3MP > 22DMB > 23DMB. In a mixture, it is entropically more favorable to adsorb more molecules with a smaller effective size. In one-dimensional channels (when all the isomers are able to fit in), the isomer with the smallest effective length will be preferentially adsorbed under saturation conditions. Note that 3MP has two configurations that are very close in energy (less than 1 kJ mol^{-1} difference in the gas phase in favor of the isomer in brackets), but that the more compact isomer is favored in adsorption, owing to more favorable vdW interactions.

We use AFI as an example of a length-entropy system. Following the method of Schenk et al.,[57] we first measured the effective length of hexane isomers. The results are provided in Table 4 and, at infinite dilution, these lengths agree well with the molecular shadow length given in Table 3. These differences in channel occupation translate immediately to different saturation loadings, with the most compact molecule having the highest saturation loading. The pure component isotherms of hexane isomers in AFI are shown in Figure 11. If a structure has channels large enough to accommodate di-branched isomers, while still inducing a parallel adsorption arrangement of the adsorbates, then the sorption hierarchy of that structure

Table 4. Molecular properties of hexane isomers in AFI at 300 K: molecular projected lengths along the channel axis at different fugacities, enthalpy of adsorption at infinite dilution. The lengths are the end-to-end distance taken along the channel axis with 3.76 Å added for vdW radius of CH_3.

Adsorbate	*L* [Å] 0 Pa	*L* [Å] 10^4 Pa	*L* [Å] 10^8 Pa	Infinite dilution properties [kJ mol^{-1}] ΔG_0	ΔH_0	$-T\Delta S$
23DMB	6.54	5.35	4.67	−33.8	−49.3	15.5
22DMB	6.63	6.33	6.29	−31.0	−46.3	15.3
3MP	7.59	6.32	4.74	−30.9	−46.9	16.0
2MP	8.12	7.39	6.33	−30.5	−47.2	16.6
*n*C6	9.28	8.62	6.85	−28.9	−44.8	16.0

© 2015 Wiley-VCH Verlag GmbH & Co. KGaA, Weinheim

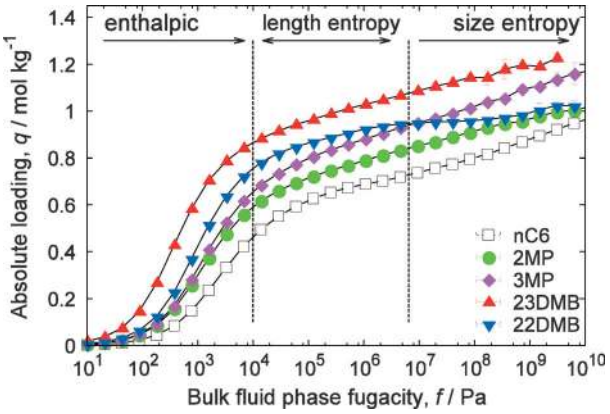

Figure 11. Single-component isotherms of C6 isomers at 433 K in AFI.

will be di-branched > mono-branched > linear. This is simply because the linear isomers will occupy the largest segment of the channel, as compared to the other isomers, whereas the di-branched isomers (the most compact ones) can arrange a larger number of molecules in the same given channel segment.[113,126,127]

Note that the concept of length entropy is limited to small pores and that the effective length depends on pressure. By increasingly compressing the molecules, for example in AFI at 10^8 Pa (see Table 4), the adsorbates reorientate and can change their internal configuration.[57] In Figure 11, we see that, at high pressure, 3-methylpentane (3MP) wins over 22-dimethylbutane (22DMB), that is, in the limit of high pressure, size entropy is dominant. Jiang and Sandler studied the length and configurational effects in carbon nanotubes as a function of channel size.[128] In the smallest channel, only the linear alkane can adsorb, excluding all branched molecules. In slightly larger channels, the adsorption order was neoC5 > *i*C5 > *n*C5, owing to length entropy. But, for even larger channels, the order is *n*C5 ≥ *i*C5 > neoC5.

Length entropy occurs when there is a difference in the saturation loading arising from the difference in the effective length of the molecules in the structure. It relies on molecules being restricted to adsorb only in certain configurations; therefore, a one-dimensional channel confinement is a requirement. Some typical examples of one-dimensional nanoporous materials that can accommodate linear and branched alkanes are AFI, FER, MAZ, MOR, and LTL. Schenk et al. computed thermodynamic properties (ΔG, ΔH, and ΔS) for (branched) alkanes in many one-dimensional channel systems and showed that length entropy drives the isomerization reaction toward the effective, most compact, isomer.[56] These entropy (stacking) effects only occur at high loadings, in which adsorbate–adsorbate interactions are important. These authors provided a thermodynamic explanation for the high branched-paraffin yield in *n*-C16 hydroconversion. Adsorption entropy not only affects the activity, but also the selectivity of many zeolite-catalyzed conversions. Shape selectivity states that molecules will not (trans-)form if they are too bulky to fit inside a channel of a zeolite. Inverse shape selectivity was proposed by Santilli et al.[129] to explain the high yield of di-branched alkanes in AFI-type of zeolites, who stated that molecules that have an optimal fit within the channels are those that form. Schenk et al. demonstrated that the molecular basis of inverse shape selectivity is related to entropic effects inside the zeolite pores under conditions where the zeolites are (almost) fully saturated.[57]

5.4. Configurational Entropy

Knowledge of branched alkanes in silicalite was limited in the 1990s, although a few experimental studies were published.[130–133] The peculiar isotherm shapes of branched alkanes in MFI were highlighted by Vlugt et al.[118] through simulations. This is mainly because, in the range of experimentally accessible pressures, the longer di-branched alkanes do not exceed four molecules per unit cells. The simulations could cover a vast range of pressures and unearthed the generic shape of the isotherms. These authors provided a molecular mechanism (by using snapshots), in which the di-branched molecules sit in the intersections of MFI, and significant additional pressure is required to push them into the zig-zag and linear channels. It was soon realized that this entropy effect could be exploited to separate linear from mono-branched alkanes in the C5–C7 carbon range,[64] and more generally to separate linear, mono-branched, and di-branched molecules.[111] In a mixture, the branched molecules are squeezed out from the silicalite and replaced with linear alkanes. This squeezing-out effect was found to be entropic in nature; the linear alkanes have a higher packing efficiency. This configurational effects was later studied in more detail[126,134–136] and also experimentally verified.

The MFI zeolite is a 3D channel system with different types of channels: 1) linear channels, 2) zig-zag channels, and 3) intersections (see Figure 1 b). The zig-zag channel is slightly wider than the linear channel; the zeolite atlas lists the maximum diameter of a sphere that can diffuse through the zig-zag channel as 4.70 Å, and the diameter of the linear channel as 4.46 Å, respectively.[137] The linear, mono-branched, and di-branched molecules have very different interactions with each of the three types of adsorption sites. The channels of MFI are 10-rings, but can expand somewhat upon adsorption, allowing more bulky molecules like di-branched alkanes and even aromatics to adsorb. However, a linear alkane is energetically and entropically favored over a mono-branched molecule and even more strongly favored over a di-branched molecule at the channel site. Vlugt et al. confirmed the entropic origin by performing simulations, using a hard-sphere model.[111] Figure 6 a shows that the replacement of branched molecules with linear molecules is mostly caused by entropy, but also (albeit much less) by the energetics.

In Figure 12, we show the pure and 5-component equimolar mixture isotherm for hexane isomers in MFI. The inflections at four molecules per unit cell in the pure component isotherms are related to the number of intersections (four per unit cell). Below the inflection, the adsorption sites for branched molecules are only the intersections. It takes significant pressure to push them into the linear and zig-zag channels. In a mixture,

© 2015 Wiley-VCH Verlag GmbH & Co. KGaA, Weinheim

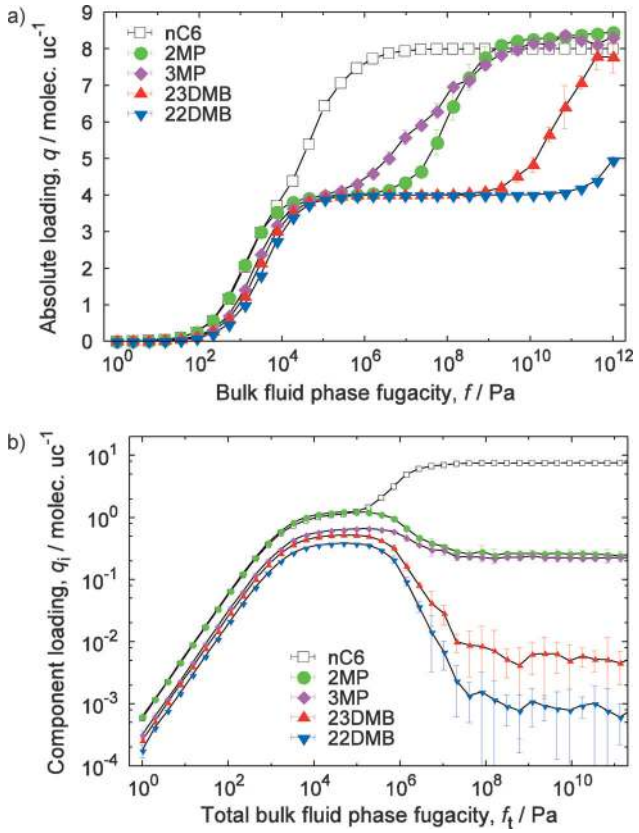

Figure 12. Configurational entropy of hexane isomers in MFI at 300 K: a) pure-component isotherms and b) component loadings in a five-component equimolar mixture as a function of loading.

competition between the isomers drives the di-branched molecules out first, with respect to the linear and mono-branched molecules. The behavior of the mono-branched molecules is between that of the linear and di-branched molecules.

Even a mixture of C5, C6, and C7, which differ in chain length, will be ordered according to the degree of branching at medium-to-high pressures.[113] In Figure 13, we show a 13-component equimolar mixture of C5–C7 isomers. The molecules now differ in degree of branching and size, leading to three regimes:

1. The enthalpic regime, in which molecules hardly interact and the hierarchy is determined by the affinity of the molecules with the framework.
2. The configurational entropy regime, in which linear molecules replaces mono-and di-branched alkanes, and mono-branched alkanes replace di-branched alkanes (the hierarchy is determined by the degrees of branching).
3. The size entropy regime , in which the molecules with the smallest size wins (the hierachy is determined by the size of the molecules).

Note that the crossover points are hard to determine, because it is not immediately clear from the figure which species replaces another one. However, *n*C5 has an inflection that is clearly caused by configurational entropy, and the start of the

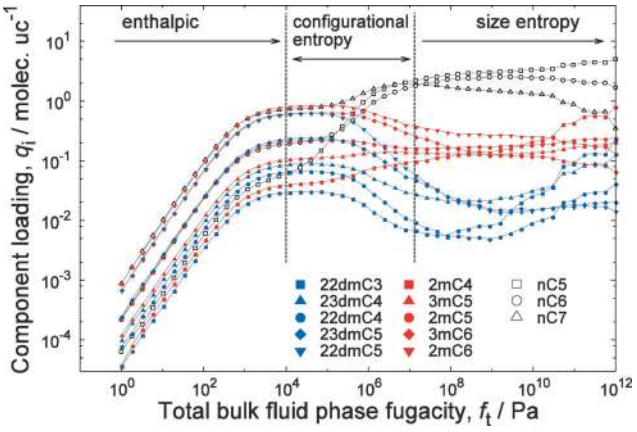

Figure 13. Relationship between enthalpy, configurational entropy, and size entropy: 13-component equimolar mixture of C5–C7 isomers at 433 K in MFI. In the enthalpic regime, the molecules do not strongly interact. In the configurational entropy regime, the linear molecules start to replace the mono- and di-branched alkanes, and the mono-branched start to replace the di-branched alkanes. Inevitably, size entropy prevails at high pressures.

influence of size entropy is around the point where *n*C7 decreases (as this can not be caused by configurational entropy which favors linear molecules over branched species; instead, this is because C5 is smaller than C7). In the limit of high pressure, size entropy will dominate. Also, because of the interplay between the three different effects, the loading of a molecule in the mixture can go up, then down, and then up again.

Configurational entropy is observed in 3D structures of channels with intersections. Figure 6a shows that, for di-branched alkanes, the forced relocation from the intersection site to the channel site results in an unfavorable entropy change. The linear hexane molecule shows the opposite trend, and its relocation results in a favorable entropy contribution. However, configurational entropy is generic in the sense that any structures with multiple sites that strongly differ in energetics and local topology/structure (i.e. the volume accessible to the adsorbate) could potentially be exploited for separations.

5.5. Commensurate Stacking

ortho-Xylenes in MIL-47 have a very effecient stacking arrangement.[138–140] They form two layers of molecules that are sandwiched between two walls. The arrangement was later coined commensurate stacking by Krishna and van Baten.[141] They also noted that a similar bookshelf structure is afforded by Co(BDP), and predicted that this MOF could, therefore, have the potential to separate C8 hydrocarbon mixtures. The Co(BDP) channel dimension of about 10 Å is close to the length of *para*-xylene, but larger than the length of *ortho*- and *meta*-xylene. *para*-Xylenes could, therefore, potentially stand upright, like a book in a bookshelf, adsorbed at the wall with its methyl groups favorably interacting with both the floor and the ceiling.

Figure 14a shows the concept of stacking of *ortho*- and *para*-xylene in a manner commensurate with the framework. A

© 2015 Wiley-VCH Verlag GmbH & Co. KGaA, Weinheim

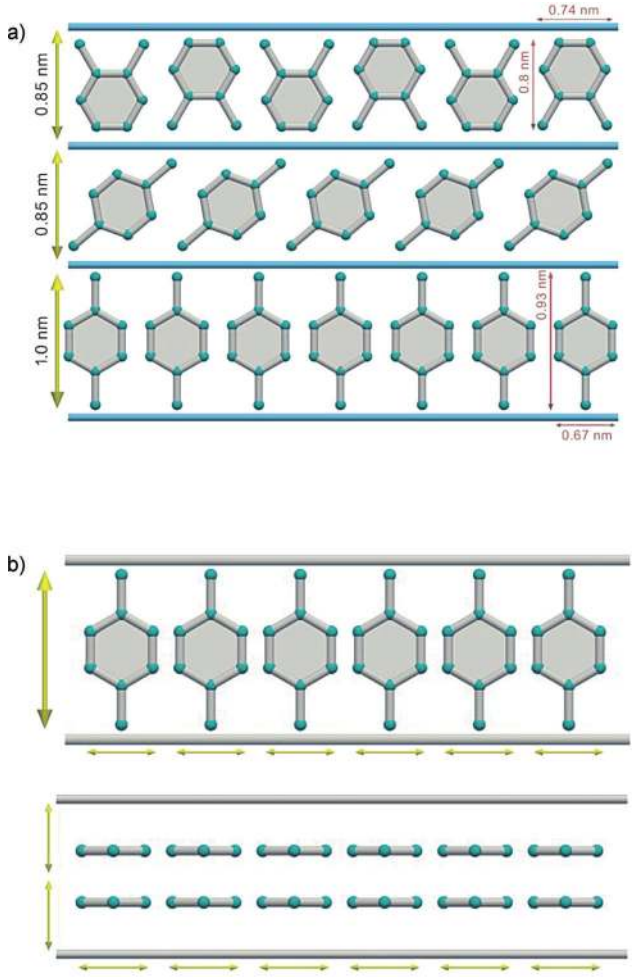

Figure 14. Schematic of commensurate stacking of xylenes in rectangular channels. a) The molecule has to be of the right size and b) an ideal *para*-xylene structure would form a double layer where the adsorbate is commensurate with the framework in all directions. The yellow arrows denote the characteristic length of the molecules, which have to be commensurate with the channel dimensions.

structure with 8.5 Å channels is commensurate with *ortho*-xylene. The structure would be *ortho*-xylene selective, because *para*-xylene cannot be stacked upright. It would have to align obliquely, thereby increasing its effective size, hence having a lower saturation loading. For *para*-selective structures, we need a channel dimension of about 10 Å. Then, *para*-xylene is able to make use of all available pore volume with both methyl groups strongly interacting with the framework.

Torres-Knoop et al. realized the potential for commensurate stacking, but formulated stronger geometric requirements.[142] Firstly, if nothing is anchoring the molecules to the wall, then the obtained configurations will be too disordered and will not exhibit the desired array of upright molecules. Therefore, a periodic anchoring along the channel direction commensurate with the width of the xylene would be required. This anchoring should be just enough to hold the molecules in place, but not so strong to impede diffusion. Secondly, a cuboid channel allows xylene to adsorb at opposite walls, but in this arrangement the ceiling and floor are blocked at that channel position (only the rotated orientation can fit, but this means disorder and a larger channel-length occupation of the xylene). As the empty space between the molecules would be wasted (and leads to too much disorder), it would be better to have a rectangular channel with the adsorbates forming layers. Idealized stacking for *para*-xylene would schematically look like Figure 14b. For molecules with different dimensions (*meta*- or *ortho*-xylene, benzene, and ethylbenzene) four effects occur:

- Wider molecules (e.g. *ortho*- and *meta*-xylene) will be able to stack less molecules per channel length.
- Longer molecules (e.g. ethylbenzene) have to align obliquely and, therefore, fewer molecules can stack per channel.
- Shorter molecules (e.g. *ortho*- and *meta*-xylene) will have less optimal interactions with the pore structure.
- More bulky and non-flat molecules (e.g. ethylbenzene) are unable to form commensurate layers and will, therefore, have a lower saturation loading. That is, commensurate stacking also provides a mechanism to separate flat from not-flat molecules. MIL-47 is particularly effective at separating styrene from ethylbenzene.[143]

In Section 6.2, we will discuss commensurate stacking in more detail.

5.6. Orientational Entropy (Pringling)

Aromatics have a particular shape; their height is much smaller than their respective length and width. Torres-Knoop et al. exploited the flatness by selecting channels of such a size that one of the isomers is able to change its orientation perpendicular to the channel.[144] The other isomers remain mostly parallel to the channel and occupy more channel space per channel length. The selected component that is able to reorientate at high loading has a significantly higher saturation capacity than its isomers. The packing of this component is reminiscent of the configuration of chips in the Pringles snack.

The concept is explained in Figure 15. As long as one can avoid molecules packing side-by-side in the channel (as would occur in rectangular channels), the effective channel occupancy can be significantly reduced by reorienting the adsorbate. To use pringling for separations, ideally only one of the isomers must be able to reorientate. Aromatics pack particular well, because their rigidity prevents internal configuration changes (as happens with flexible alkanes in length entropy). In Section 6.3, we will show that high selectivities in large pores can be obtained for very complicated mixtures. Ellipsoid or diamond-shaped channels could potentially be *para*-xylene selective.

5.7. Discussion of Entropic Separation Mechanisms

It is, in principle, always possible to separate molecules that differ in size by using size entropy. The principle does not dependent on the difference in adsorption energetics, but the crossover point at which entropy wins is dependent on many factors. As experimental equipment and industrial setups are limited in terms of pressure, the entropy effect might not always be usable in practice for molecules that differ too much

© 2015 Wiley-VCH Verlag GmbH & Co. KGaA, Weinheim

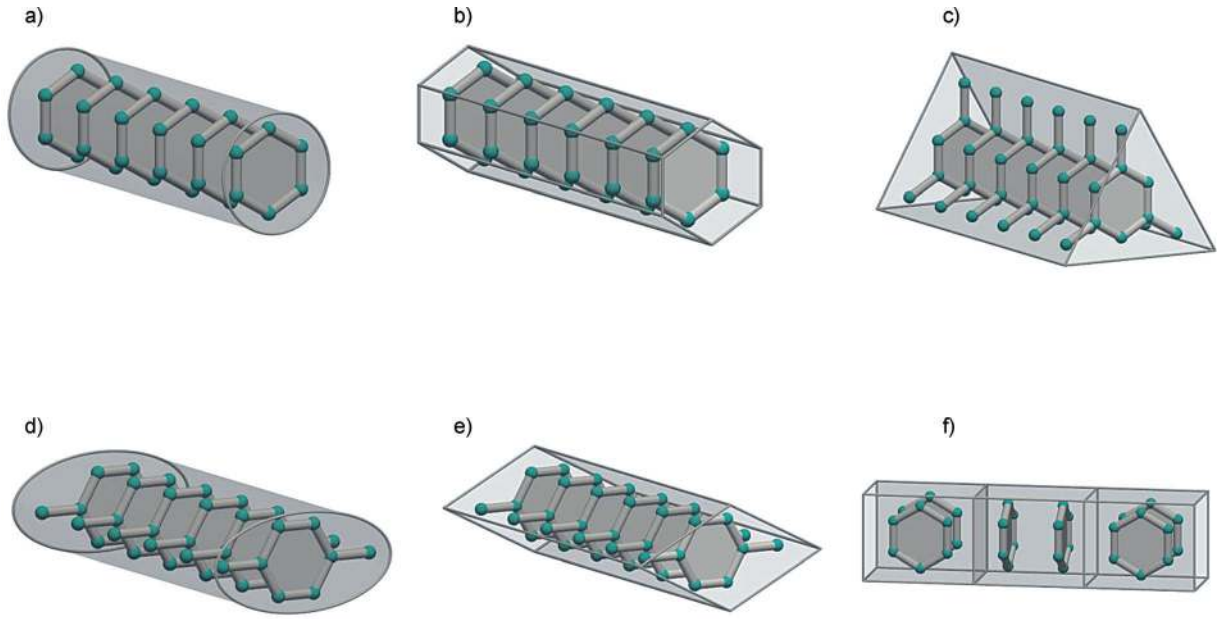

Figure 15. Orientational entropy (pringling): an ideal and tightly packed arrangement of molecules that have a shape commensurate with the channel. a) Cylindrical channels for circular molecules (e.g. benzene), b) honeycomb channels for hexagonal molecules (e.g. benzene), c) triangular channels for triangular molecules (e.g. cyclopropane, mesitylene, aluminumhydroxide). Perhaps d) elliptical or e) diamond-like channels will be found that allow *para*-xylene to pringle. In pringling, one of the components is able to align perpendicular, while the other isomers are unable to stack this way and have a significant lower saturation loading. This concept leads to efficient separations, especially near pore-saturation conditions. Not all shapes are optimal, for example in (f) cuboid or rectangular channels have no discrimination between the parallel and perpendicular orientation and no difference in saturation loading would occur.

in size (and hence the adsorption affinity that has to be overcome).

The other entropy effects can be applied to isomers, which usually have similar adsorption affinities for the framework, but also to mixtures that differ in molecular size. The ranges over which the size can vary depend on the particular system and on the affinity of the molecules for the framework. Commensurate stacking is the most sensitive of these to the low-loading part, as the saturation loadings of the isomers can be the same for some of the components. It is both an enthalpic and entropic mechanism.

All discussed entropy effects share one important feature, that is, the effective smallest mixture component wins at high pressure. They differ in the details of how this size reduction is achieved. Packing usually refers to arrangements of molecules amongst themselves. In adsorption, it also refers to arrangements of pockets of molecules in nanoporous cavities. Stacking is often used for arrangements of molecules with colinear alignment of, for example, the dipole moment. In nanoporous materials it refers to regular arrangements of molecules induced by the framework (they stack with respect to the framework). In nanoporous materials, it is often possible to view entropy as being related to the amount of molecules per effective channel length. Sometimes, this is denoted by the term smallest footprint. For example, in pringling, the footprint is reduced from one of the two largest dimensions to its smallest size. This can easily lead to an increase in saturation capacity by a factor of 2, and hence a huge gain in separation efficiency.

6. Applications (Entropic Separations)

In this section, we will explain the entropic separation mechanisms with concrete examples, which allow us to discuss the underlying physics in more detail.

6.1. Linear/Branched Alkanes

Di-branched alkanes in the C5–C7 range are preferred components of high-octane gasoline. Therefore, the separation of linear, mono-branched, and di-branched molecules is of significant importance in the petrochemical industry. Separations that use nanoporous materials provide an alternative to the PENEX/DIH technology, which achieves a near-complete production of di-branched molecules for C5/C6 feedstocks, but not for C6/C7 feedstocks. To screen structures for gasoline applications, it is sufficient to examine C6 and C7. Usually, C5 is excluded from the analysis, as nearly all isopentane is mono-branched in the feedstock.

In industry, catalytic isomerization is used to convert linear molecules to branched molecules. After isomerization, the resulting mixture of isomers requires separation and recycling of the non-isomerized components. Traditionally, the Isosiv process (using LTA-5A zeolites) is employed to separate linear alkanes from the mono-branched through sieving (the 8-ring windows of LTA only allow linear alkanes to pass). In this setup, non-optimal mono-branched molecules would be collected with the di-branched molecules as the products. A more efficient approach is shown in Figure 16. Here, only the desired di-branched molecules are separated as the product, whereas

© 2015 Wiley-VCH Verlag GmbH & Co. KGaA, Weinheim

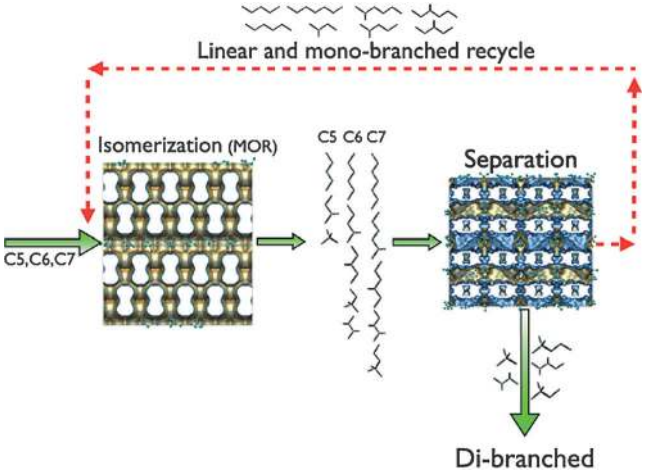

Figure 16. Schematic of the separation process. The feed consists of mostly linear alkanes. First, the linear alkanes are isomerized to branched alkanes (usually using MOF-zeolite). Next, the linear and mono-branched alkanes are separated from the desired di-branched alkanes and recycled back.

the linear and mono-branched alkanes are recycled back to the isomerization unit.

Recently, Dubbeldam et al. computationally screened more than 100 zeolites, MOFs, and ZIFs to find an optimal structure to be used in the separation step.[145] Figure 17 summarizes the screening data and illustrates many important points. In general, the selectivity and pore size are inversely related. With larger pores, you have more fluid per framework volume, but this is at the expense of the selectivity. In the small pore range, high selectivities can be achieved. ZIF-77 and $Fe_2(BDP)_3$ have separation factors $\gg 100$. The adsorption selectivity is defined as the loading of the linear + mono-branched molecules divided by the loading of the di-branched molecules (times a factor of 2/3 for an equimolar mixture), when the linear molecules adsorb the most. The reverse hierarchy can be also found, in which the opposite ranking is observed (the di-branched molecules adsorb the highest, then the mono-branched, and the linear molecules the lowest). Similarly, the adsorption selectivity is then defined as the loading of the di-branched divided by the loading of the linear + mono-branched alkanes (times a factor 3/2 for an equimolar mixtures to take the different number of components of the di-branched vs. linear species into account).

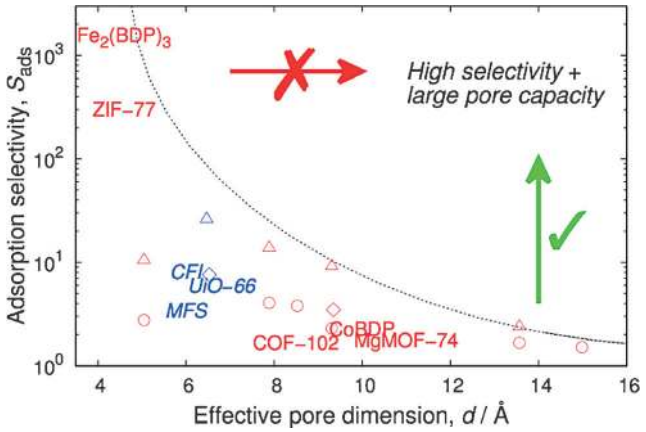

Figure 17. Alkane adsorption separation selectivity at 100 kPa and 433 K. Red color denotes the normal hierarchy (linear > mono-branched > di-branched), and blue color denotes the reverse hierarchy (di-branched > mono-branched > linear).

UiO-66 is an example with a reverse ranking. As can be seen in Figure 17, all of the reverse hierarchy structures have pore dimensions of about 6 Å. For shorter or larger pores, we find normal hierarchy. This is not coincidental, but, before discussing the underlying cause, it is important to determine what ranking would be preferred. The total selectivity is determined by the adsorption selectivity and the diffusion selectivity. The diffusion selectivity for alkanes in nanoporous materials is generally in favor of linear molecules, which diffuse much faster than the more bulky mono-branched and di-branched molecules. This means that, for the normal hierarchy, diffusion effects enhance the adsorption selectivity, whereas, for the reverse hierarchy, diffusion effects impede the adsorption selectivity.

The normal hierarchy can be found for small pore channels and larger pore channels. Both are useful for different purposes. For example, ZIF-77 and $Fe_2(BDP)_3$ have such high selectivities that they are capable of fractionating feed stocks into their individual components. Figure 18 shows a pulse-breakthrough simulation of a 13-component equimolar mixture of C5–C7 isomers. Even for chains that differ in chain lengths, the order is that first the di-branched molecules come out, then the mono-branched, and lastly the linear molecules. Note that these groups of peaks are separated without any overlap, meaning that high purities can be obtained without recycling. The normal hierarchy for larger pores have low(-er) selectivities, but are useful for efficiently treating large amounts of fluid without the rigorous need for pure products.

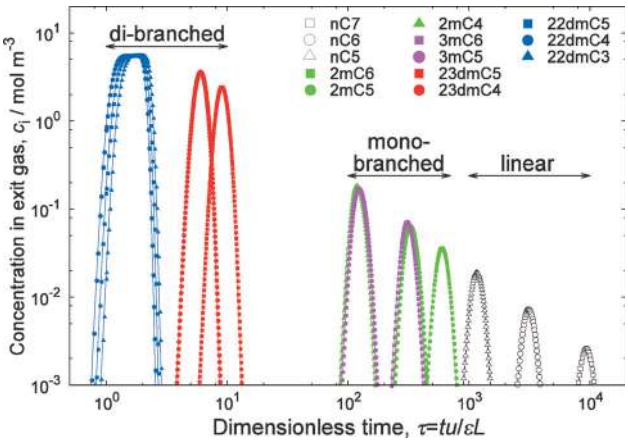

Figure 18. Simulated pulse-style breakthrough curves of C5–C7 isomers in ZIF-77 at partial fugacities of the bulk-fluid phase of 20 kPa and 433 K. The pulse-style breakthrough clearly shows that ZIF-77 is able to fractionate the individual components of a C6 mixture, and when it is fed an alkane mixture differing in chain length, it is still able to fractionate the mixture into linear, mono-branched, and di-branched components.

© 2015 Wiley-VCH Verlag GmbH & Co. KGaA, Weinheim

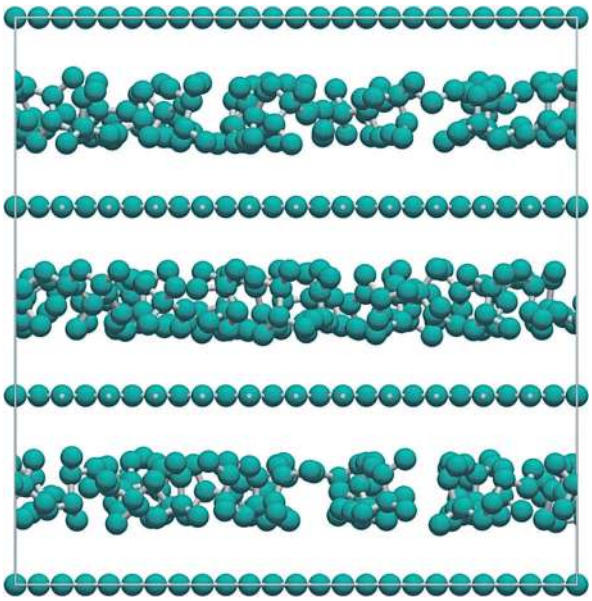

Figure 19. Graphite layer system with tunable layer spacing. The image shows an equimolar C6 isomer mixture in a 6.5 Å layer spacing at a total fugacity of the bulk-fluid phase of 100 kPa and at 433 K.

The simulations were able to elucidate the underlying mechanism of alkane adsorption, following Severson and Snurr's methodology of studying alkanes in a simplified system.[146] Figure 19 shows a periodic sheet system, in which the distance between the sheets can easily be adjusted. Dubbeldam et al. used a cuboid channel, because, in nanoporous materials, the adsorbates are at least confined in two dimensions. The system is small and simple enough to accurately compute properties such as the heat of adsorption of a single molecule. The difference between linear, mono-branched, and di-branched molecules is striking (Figure 20). At small and large wall distances, the linear molecule is energetically favored. In fact, at small distances the differences can be very large, because of size exclusion, where the di-branched molecules, in particular, barely fit. This explains why the selectivites for the ZIF-77 and $Fe_2(BDP)_3$ are so high, and why we find a linear hierarchy at larger distances. We also observed that the only regime in which the order of di-branched and linear molecules is reversed is around 6 Å (exactly where we found all the reverse-hierarchy structures in the screening study; Figure 17).

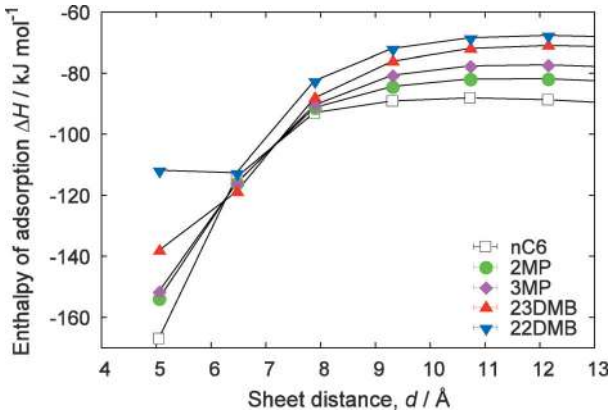

Figure 20. Enthalpy of adsorption of hexane isomers in square graphite channels at 433 K and infinite dilution.

This result is in agreement and related to the previously discussed findings of Schenk et al.[56,57] regarding the optimal size of channels for linear versus branched alkanes, and the change in selectivity as a function of carbon nanotube size by Jiang et al.[128]

The large-pore systems have a dominant entropy contribution. The goal would be to combine high selectivity with high pore capacity (top-right of the graph). It is not possible to have isomer discrimination based on energetics and extend that to higher pore sizes. After all, the reason for this high selectivity is the strong channel confinement. In the next section, we will show that it is possible, however, to exploit entropy effects to increase the selectivity of large-pore systems.

6.2. BTEX Separation Process

The separation of C8 aromatic hydrocarbons is of great importance in the petrochemical industries. Xylenes are obtained from petroleum and generally produced as a mixture of three isomers, that is, *ortho*-, *meta*-, and *para*-xylene, with methyl groups attached to the aromatic ring in positions 1-2, 1-3, and 1-4, respectively (see Figure 21). The acronym BTX refers to mixtures of benzene, toluene, and the three xylene isomers. If ethylbenzene is included, the mixture is often referred to as BTEX. *para*-Xylene is the most valuable of the isomers. It is primarily used as a feedstock with purity requirements of 99%+ for terephthalic acid or dimethyl terephthalate production,

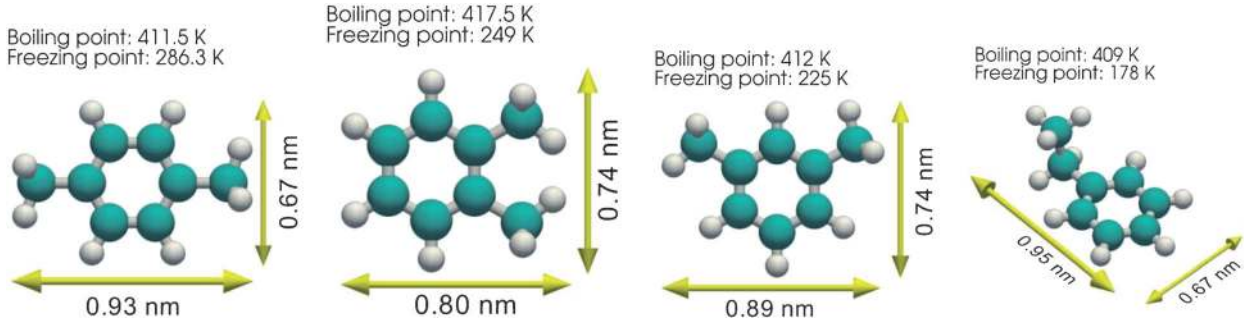

Figure 21. Properties of xylenes: a) *para*-xylene, b) *ortho*-xylene, c) *meta*-xylene, and d) ethylbenzene.

© 2015 Wiley-VCH Verlag GmbH & Co. KGaA, Weinheim

whose uses include polyester fibers and polyethylene terephthalate (PET) resins for beverage bottles. Owing to the small differences in boiling points, it is difficult to separate *para*-xylene from *meta*- and *ortho*-xylene. In principle, crystallization can be used to make use of the larger differences in freezing points. These differences arise because of the differences in stacking efficiency of the molecules. *para*-Xylene has the highest freezing point and is the first to emerge from the solution. However, the energy requirements for fractional crystallization are high, because of the need to cool to temperatures of about 220 K. Selective adsorption of xylene isomers by using nanoporous materials is an energy-efficient alternative to crystallization. Currently, Ba-X zeolite adsorbents are used in UOP Parex and IFP Eluxyl technologies. Currently, one of the best performing MOFs is the strongly *ortho*-selective MIL-47 structure.[139, 140, 147]

To design and find structures that could perform better, we should look for structures that: 1) are highly *para*-xylene selective, 2) have a large capacity, and 3) make use of that large pore volume by operating at, or near, saturation conditions. Torres-Knoop et al. screened for commensurate stacking and focused on structures with pore dimensions around 10 Å.[142] Two structures were highlighted that indeed showed commensurate stacking: 1) MIL-47 for *ortho*-xylene and 2) MAF-X8 for *para*-xylene. Figures 22 a and 22 b show snapshots from a simulation at saturation conditions. The one-dimensional, lozenge-shaped, rhombohedric channels of MIL-47 offer the appropriate bookshelf that is required to optimally stack *ortho*-xylenes. The channels of MIL-47 are not large enough to allow *para*-xylene to stack upright; these molecules have to align obliquely along the channel length. Hence, MIL-47 is strongly *ortho*-selective. MAX-X8, a Zn(II) pyrazolate–carboxylate framework, possesses the right channel dimensions for the stacking of *para*-xylene to occur. Figure 22 clearly shows the regular array of *para*-xylene molecules stacked in two layers. The commensurate stacking of *ortho*-xylene in MIL-47 is close to optimal, whereas the stacking of *para*-xylene in MAF-X8 is suboptimal. The molecules are somewhat tilted in an alternating arrangement, owing to the tortuosity of the MAF-X8 channel. There is, therefore, room for improvement.

The isotherm of the equimolar mixture in MAF-X8 confirms its strong *para*-xylene selectivity (Figure 23). The ideal adsorption solution theory (IAST) predicts the isotherm of the mixture based on the pure components and is found to be in excellent agreement. The mixture shows high *para*-xylene selectivity combined with a high *para*-xylene loading in the mixture (about 2.2 mol kg^{-1} at 1 bar).

Figure 24 summarizes the efficiency of all structures that were included in the screening study and found to be *para*-selective. In Figure 24, the adsorption selectivity is plotted versus the *para*-xylene loading in the mixture. This plot is conceptually similar to Figure 17 for alkanes. Usually, adsorption selectivity and the *para*-xylene loading (i.e. pore capacity) are inversely related. But, surprisingly, MAF-X8 has achieved nearly the same separation selectivity as Ba-X, but at a much higher pore capacity. When Figure 24 is compared to Figure 17, one should take into account that the separation factors for xylenes are, in

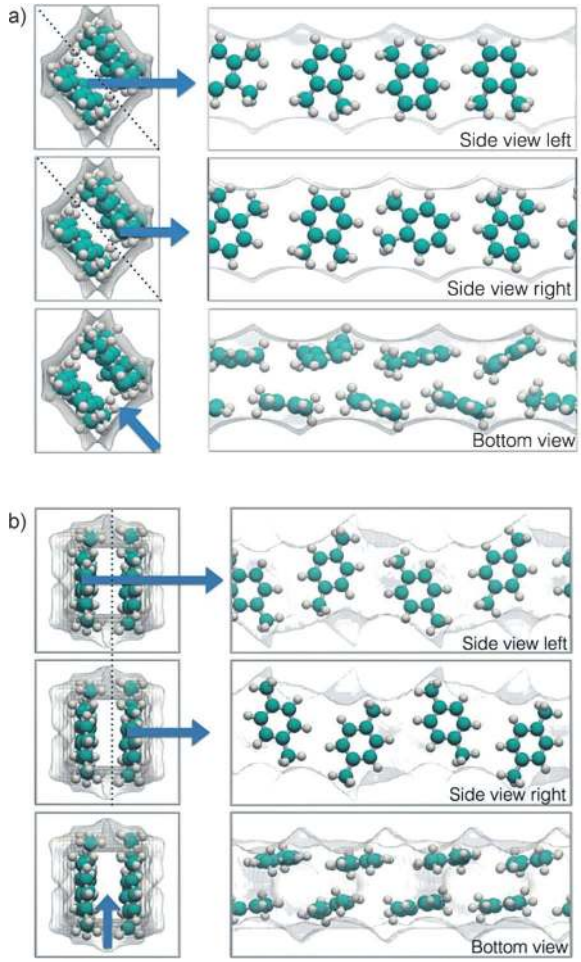

Figure 22. Commensurate stacking. a) Stacking of *ortho*-xylene in MIL-47.[140, 142] The snapshot is taken from a simulation at 433 K and saturation loading. The 8.5 Å channels of MIL-47 are perfect for optimally stacking *ortho*-xylenes. b) Stacking of *para*-xylene in the MAF-X8 structure.[142] Note that the xylene is commensurate in three dimensions, that is, it fits perfectly length-wise, it forms two layers that fit snugly, and it stacks in an alternating fashion along the channel.

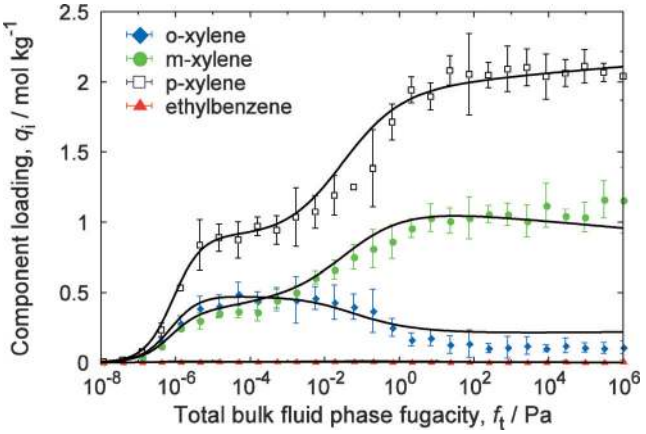

Figure 23. Isotherms at 433 K of a BTEX equimolar mixture and IAST prediction based on pure components.

© 2015 Wiley-VCH Verlag GmbH & Co. KGaA, Weinheim

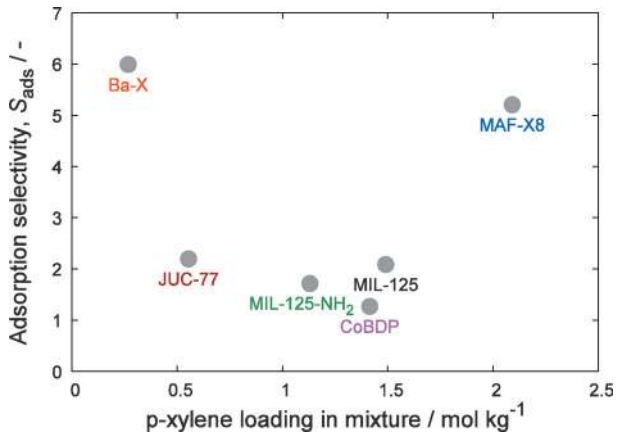

Figure 24. Comparison of *para*-xylene-selective MOFs: adsorption selectivity versus *para*-xylene capacity.

general, much lower than for alkanes. Nonetheless, commensurate stacking is able to combine high pore capacities with sufficient adsorption selectivities (for this system). Note that MIL-125, MIL-125, and JUC-77 have small pores, and their adsorption selectivities would be significantly diminished when diffusion is taken into account. For MAF-X8, we expect no, or limited, diffusional limitations.

6.3. Face-to-Face Stacking

In the previous section, we showed how commensurate stacking was able to increase the adsorption selectivity at high pore capacities. In this section, we show a second example, namely, the exploitation of orientational entropy effects for aromatics in one-dimensional channels.[144] In this case, very high separation factors can be combined with very high pore capacities.

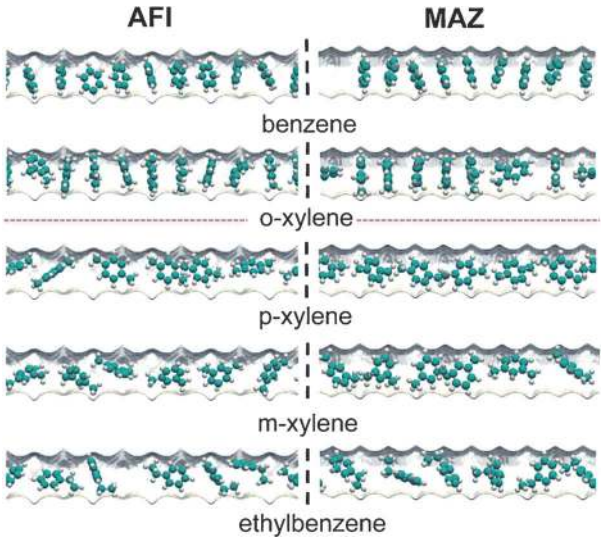

Figure 25. Snapshots of benzene, *ortho*-, *para*-, and *meta*-xylenes, as well as ethylbenzene in AFI and MAZ unders saturation conditions. At high loadings, benzene and *ortho*-xylene form pringle stacking, thereby significantly reducing their footprint compared to *para*- and *meta*-xylene as well as ethylbenzene.

The reorientation entropy can best be explained with snapshots. In Figure 25, we show snapshots of benzene as well as *ortho*-, *para*-, and *meta*-xylene in AFI and MAZ channels at saturation conditions. The AFI zeolite possesses one-dimensional channels with corrugated pore topology; the channel diameter at the narrow constrictions is 7.3 Å and at the protracted segments is 8.4 Å. MAZ zeolite is slightly smaller than AFI; the channel diameters at the narrow and protracted segments are 6.7 and 7.4 Å, respectively. The height and width of *ortho*-xylene are both smaller then 8.4 and 7.4 Å, allowing a perpendicular arrangement with respect to the channel axis within the protracted segments in both AFI and MAZ. For *meta*- and *para*-xylene as well as ethylbenzene, either the height or width are too large to allow vertical alignment. Consequently, their orientations within the channels are oblique.

AFI is a strongly ortho-xylene selective structure (see breakthrough simulations in Figure 26). The origin of the ortho-

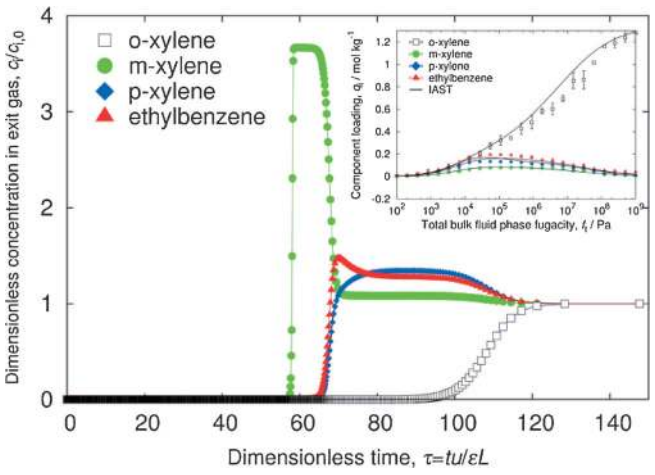

Figure 26. Breakthrough simulations at 100 kPa and mixture isotherms (inset) for an equimolar mixture of *ortho*-/*para*-/*meta*-xylene and ethylbenzene in AFI zeolite at 433 K. The reorientation of *ortho*-xylene allows higher saturation capacity and drives the other mixture components out.

xylene (and benzene) selectivity is reorientation which is not an enthalpic, but an entropic mechanism. For an enthalpic explanation, the adsorbates would have to pringle, even at low loading. During the simulations, the average orientation can be measured as a function of pressure at several points along the isotherm. At low loading, the molecules preferentially orientate parallel to the axis channel (this can be measured during the simulations, and also be confirmed by energy minimizations). When the loading is increased, the molecules start to pringle. The driving force is the pressure (i.e. chemical potential). Above 75% saturation loading, most molecules are found in a face-to-face stacking arrangement. The effect is not caused by the corrugation of the wall (even for a cylindrical channel with perfectly smooth walls the effect is found). These effects are usually of secondary importance.[57]

Having elucidated the origin, it is then a matter of searching for the right systems to exploit this effect. Torres-Knoop used the structural versatility of MOFs to create a larger version of

© 2015 Wiley-VCH Verlag GmbH & Co. KGaA, Weinheim

an existing triangular channel MOF, $Fe_2(BDP)_3$. The BDP linker was extended with an additional phenyl group to create slightly larger triangular channels (see Figure 3) that can accommodate aromatics in a perpendicular arrangement. As adsorbates, a mixture of 1,3,5- trichlorobenzene, 1,2,5-trichlorobenzene, and 1,3,5 trichlorobenzene was chosen. 1,3,5-Trichlorobenzene is triangular shaped and, hence, reorientation is possible, whereas the other two components are rotationally confined. Indeed, snapshots in Figure 27 confirmed this hypothesis. The

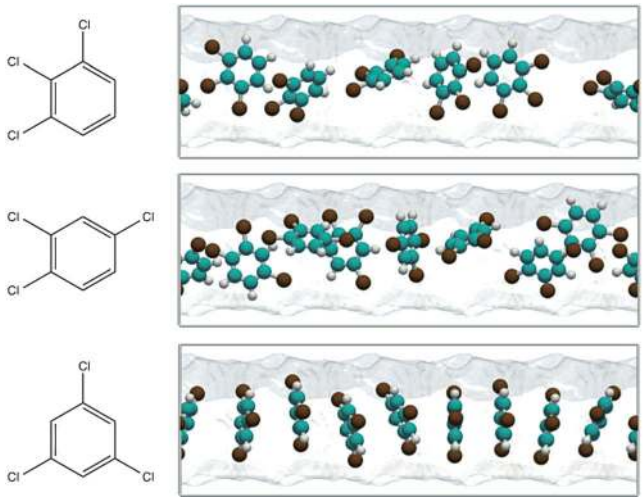

Figure 27. Snapshots of trichlorobenzene isomers in an $Fe_2(BDP)_3$ variant. The reorientation of the 1,3,5-trichlorobenzene results in a much reduced effective length (footprint) and, hence, a higher saturation capacity.

mixture isotherm of the tricholobenzene shows the promise of this type of entropic separation mechanism; the separation is extremely efficient at high capacities (Figure 28 shows a capacity of over 3.5 mol kg^{-1} at 1 bar).

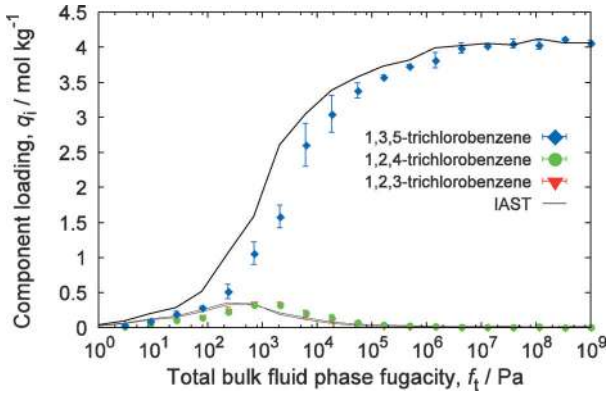

Figure 28. Mixture isotherms for 1,3,4-/1,3,6-/1,5,6-trichlorobenzene equimolar mixture in the modified $Fe_2(BDP)_3$ at 433 K. Molecules that are able to reorient in a pringle configuration have much higher saturation capacities. Differences in the saturation capacities have a strong influence on the separation performance.

7. Conclusions

This Review highlights the potential of adopting separating strategies that rely on differences in effective molecular size, rather than adsorption affinity. Size entropy is not readily extendable to large-pore structures, because the pressure that is needed to reach pore saturation can be high in MOFs. Pore saturation is needed for a smaller component to win entropically and overcome the enthalpic penalty caused by the affinity with the framework. Length and configurational entropies are linked to small-pore frameworks such as 8-, 10-, or 12-ring channel zeolites. As the effect is casued by confinement (by the framework), it is difficult to extend it to more open pores. Commensurate stacking and the orientational entropy mechanism are also attributed to confinement, but by the framework and by other adsorbates. Hence, these mechanisms are able to operate under saturation conditions in systems with large open pores (large capacity), while still achieving high selectivities. The main conclusion of this review is that the *large* pore volumes of MOFs for industrial separation applications are primarily suitable for separating *large* molecules.

Computational Details (Simulations)

The adsorption computations of single and multiple components are usually performed in the grand-canonical ensemble.[148,149] Ref. [150] reviews state-of-the-art adsorption simulation methodologies. The presented adsobent/adorbate systems can, nowadays, be accurately modeled in full atomistic detail by using calibrated classical force fields. Common force fields include TraPPE[151] and OPLS[152] for adsorbates like alkanes and xylenes, respectively, and TraPPE-Zeo,[153] DREIDING,[154] and UFF[155] for the modeling of zeolites and MOFs. By using the dual-site Langmuir–Freundlich fits of the pure component isotherms, breakthrough calculations can be carried out by solving a set of partial differential equations for each of the species in the gas mixture.[156] The molar loadings of the species at any position along the packed bed and at any time are determined from IAST calculations.

Acknowledgements

We thank T. J. H. Vlugt and S. Calero for comments and fruitful discussion, and J. Heinen and N. C. Burtch for comments on the manuscript. This work was supported by the Netherlands Organization for Scientific Research (NWO) through a VIDI grant.

Keywords: adsorption · entropy · metal–organic frameworks · molecular simulation · separations

[1] W. O. Haag, *Zeolites and Related Microporous Materials: State of the Art 1994*, Elsevier, Amsterdam, **1994**, pp. 1375 – 1394.
[2] C. Rhodes, *Sci. Prog.* **2010**, *93*, 223 – 284.
[3] S.-Y. Chui, S.-F. Lo, J. Charmant, A. Orpen, I. Williams, *Science* **1999**, *283*, 1148 – 1150.
[4] H. Li, M. Eddaoudi, M. O'Keeffe, O. Yaghi, *Nature* **1999**, *402*, 276 – 279.
[5] M. Eddaoudi, J. Kim, N. Rosi, D. Vodak, J. Wachter, M. O'Keeffe, O. Yaghi, *Science* **2002**, *295*, 469 – 472.
[6] O. Yaghi, M. O'Keeffe, N. Ockwig, H. Chae, M. Eddaoudi, J. Kim, *Nature* **2003**, *423*, 705 – 714.

© 2015 Wiley-VCH Verlag GmbH & Co. KGaA, Weinheim

[7] S. Kitagawa, R. Kitaura, S. Noro, *Angew. Chem. Int. Ed.* **2004**, *43*, 2334 – 2375; *Angew. Chem.* **2004**, *116*, 2388 – 2430.
[8] K. Park, Z. Ni, A. Côté, J. Choi, R. Huang, F. Uribe-Romo, H. Chae, M. O'Keeffe, O. Yaghi, *Proc. Natl. Acad. Sci. USA* **2006**, *103*, 10186 – 10191.
[9] D. M. Ruthven, *Principles of Adsorption and Adsorption Processes*, Wiley, New York, **1984**.
[10] J. Karger, D. M. Ruthven, D. Theodorou, *Diffusion in Nanoporous Materials*, Wiley, New York, **2012**.
[11] R. June, A. Bell, D. Theodorou, *J. Phys. Chem.* **1990**, *94*, 8232 – 8240.
[12] R. June, A. Bell, D. Theodorou, *J. Phys. Chem.* **1990**, *94*, 1508 – 1516.
[13] R. Snurr, R. June, A. Bell, D. Theodorou, *Mol. Simul.* **1991**, *8*, 73 – 92.
[14] R. Snurr, J. Hupp, S. Nguyen, *AIChE J.* **2004**, *50*, 1090 – 1095.
[15] U. Mueller, M. Schubert, F. Teich, H. Puetter, K. Schierle-Arndt, J. Pastre, *J. Mater. Chem.* **2006**, *16*, 626 – 636.
[16] R. Kuppler, D. Timmons, Q. Fang, J. Li, T. Makal, M. Young, D. Yuan, D. Zhao, W. Zhuang, H. Zhou, *Coord. Chem. Rev.* **2009**, *253*, 3042 – 3066.
[17] A. Czaja, N. Trukhan, U. Muller, *Chem. Soc. Rev.* **2009**, *38*, 1284 – 1293.
[18] S. Kitagawa, R. Matsuda, *Coord. Chem. Rev.* **2007**, *251*, 2490 – 2509.
[19] G. Férey, *Chem. Soc. Rev.* **2008**, *37*, 191 – 214.
[20] J. Long, O. Yaghi, *Chem. Soc. Rev.* **2009**, *38*, 1213 – 1214.
[21] T. Düren, L. Sarkisov, O. Yaghi, R. Snurr, *Langmuir* **2004**, *20*, 2683 – 2689.
[22] L. Sarkisov, J. Kim, *Chem. Eng. Sci.* **2015**, *121*, 322 – 330.
[23] K. Walton, A. Millward, D. Dubbeldam, H. Frost, J. Low, O. Yaghi, R. Snurr, *J. Am. Chem. Soc.* **2008**, *130*, 406 – 407.
[24] D. Dubbeldam, K. Walton, *Metal – organic Frameworks: Materials Modeling towards Engineering Applications*, Pan Stanford, New York, 2015, pp. 53 – 112.
[25] A. Shrake, J. Rupley, *J. Mol. Biol.* **1973**, *79*, 351 – 371.
[26] K. Walton, R. Snurr, *J. Am. Chem. Soc.* **2007**, *129*, 8552 – 8556.
[27] T. Düren, F. Millange, G. Férey, K. Walton, R. Snurr, *J. Phys. Chem. C* **2007**, *111*, 15350 – 15356.
[28] O. Talu, A. Myers, *AIChE J.* **2001**, *47*, 1160 – 1168.
[29] S. Han, J. Mendoza-Cortes, W. Goddard, *Chem. Soc. Rev.* **2009**, *38*, 1460 – 1476.
[30] Y. He, W. Zhou, G. Qian, B. Chen, *Chem. Soc. Rev.* **2014**, *43*, 5657 – 5678.
[31] H. Langmi, J. Ren, B. North, M. Mathe, D. Bessarabov, *Electrochim. Acta* **2014**, *128*, 368 – 392.
[32] J. Liu, P. Thallapally, P. McGrail, D. Brown, J. Liu, *Chem. Soc. Rev.* **2012**, *41*, 2308 – 2322.
[33] G. Férey, C. Serre, T. Devic, G. Maurin, H. Jobic, P. Llewellyn, G. DeWeireld, A. Vimont, M. Daturi, J. Chang, *Chem. Soc. Rev.* **2011**, *40*, 550 – 562.
[34] J.-R. Li, Y. Mas, M. McCarthy, J. Scully, J. Yu, H.-K. Jeon, P. Balbuena, H.-C. Zhou, *Coord. Chem. Rev.* **2011**, *255*, 1791 – 1823.
[35] T. Düren, Y. Bae, R. Snurr, *Chem. Soc. Rev.* **2009**, *38*, 1237 – 1247.
[36] J.-R. Li, J. Sculley, H.-C. Zhou, *Chem. Rev.* **2012**, *112*, 869 – 932.
[37] J. Lee, O. Farha, J. Roberts, K. Scheidt, S. Nguyen, J. T. Hupp, *Chem. Soc. Rev.* **2009**, *38*, 1450 – 1459.
[38] D. Farrusseng, S. Aguado, C. Pinel, *Angew. Chem. Int. Ed.* **2009**, *48*, 7502 – 7513; *Angew. Chem.* **2009**, *121*, 7638 – 7649.
[39] L. Ma, W. Lin, *Top. Curr. Chem.* **2009**, *293*, 175 – 205.
[40] P. Valvekens, F. Vermoortele, D. De Vos, *Catal. Sci. Technol.* **2013**, *3*, 1435 – 1445.
[41] J. Liu, L. Chen, H. Cui, J. Zhang, L. Zhang, C.-Y. Su, *Chem. Soc. Rev.* **2014**, *43*, 6011 – 6061.
[42] J. Cavka, S. Jakobsen, U. Olsbye, N. Guillou, C. Lamberti, S. Bordiga, K. Lillerud, *J. Am. Chem. Soc.* **2008**, *130*, 13850 – 13851.
[43] P. Bárcia, D. Guimarães, P. Mendes, J. Silva, V. Guillerm, H. Chevreau, C. Serre, A. Rodrigues, *Microporous Mesoporous Mater.* **2011**, *139*, 67 – 73.
[44] J. Israelachvili, *Intermolecular and Surface Forces*, 3rd ed., Elsevier, Amsterdam, **2011**.
[45] N. Burtch, H. Jasuja, K. Walton, *Chem. Rev.* **2014**, *114*, 10575 – 10612.
[46] S. Bhatia, A. Myers, *Langmuir* **2006**, *22*, 1688 – 1700.
[47] H. Frost, R. Snurr, *J. Phys. Chem. C* **2007**, *111*, 18794 – 18803.
[48] D. Durbin, C. Malardie-Jugroot, *Int. J. Hydrogen Energy* **2013**, *38*, 14595 – 14617.
[49] Y. Peng, V. Krungleviciute, I. Eryazici, J. Hupp, O. Farha, T. Yildirim, *J. Am. Chem. Soc.* **2013**, *135*, 11887 – 11894.
[50] A. Skoulidas, D. Sholl, *J. Phys. Chem. B* **2005**, *109*, 15760 – 15768.
[51] A. Myers, J. Prausnitz, *AIChE J.* **1965**, *11*, 121 – 127.
[52] C. Tien, *Adsorption Calculations and Modelling*, Butterworth-Heinemann, Newton, MA, USA, **1994**.
[53] A. Myers, P. Monson, *Langmuir* **2002**, *18*, 10261 – 10273.
[54] A. Myers, P. Monson, *Adsorption* **2014**, *20*, 591 – 622.
[55] G. Woods, A. Panagiotopoulos, J. Rowlinson, *Mol. Phys.* **1988**, *63*, 49 – 63.
[56] M. Schenk, S. Calero, T. Maesen, T. Vlugt, L. van Benthem, M. Verbeek, B. Schnell, B. Smit, *J. Catal.* **2003**, *214*, 88 – 89.
[57] M. Schenk, S. Calero, T. Maesen, L. van Benthem, M. Verbeek, B. Smit, *Angew. Chem. Int. Ed.* **2002**, *41*, 2499 – 2502; *Angew. Chem.* **2002**, *114*, 2609 – 2612.
[58] T. Duerinck, R. Bueno-Perez, F. Vermoortele, D. de Vos, S. Calero, G. Baron, J. Denayer, *J. Phys. Chem. C* **2013**, *117*, 12567 – 12578.
[59] J. Denayer, R. Ocakoglu, I. Arik, C. Kirschhock, J. Martens, G. Baron, *Angew. Chem. Int. Ed.* **2005**, *44*, 400 – 403; *Angew. Chem.* **2005**, *117*, 404 – 407.
[60] F. Karavias, A. Myers, *Langmuir* **1991**, *7*, 3118 – 3126.
[61] T. Vlugt, E. Garcia-Perez, D. Dubbeldam, S. Ban, S. Calero, *J. Chem. Theory Comput.* **2008**, *4*, 1107 – 1118.
[62] S. Tedds, A. Walton, D. Broom, D. Book, *Faraday Discuss.* **2011**, *151*, 75 – 94.
[63] B. Smit, T. L. M. Maesen, *Nature* **1995**, *374*, 42 – 44.
[64] R. Krishna, T. Vlugt, B. Smit, *J. Phys. Chem. A* **1998**, *102*, 7727 – 7730.
[65] D. Dubbeldam, S. Calero, T. J. H. Vlugt, R. Krishna, T. L. M. Maesen, B. Smit, *J. Phys. Chem. B* **2004**, *108*, 12301 – 12313.
[66] L. Clark, A. Gupta, R. Snurr, *J. Phys. Chem. B* **1998**, *102*, 6720 – 6731.
[67] E. J. Maginn, A. T. Bell, D. N. Theodorou, *J. Phys. Chem.* **1995**, *99*, 2057 – 2079.
[68] D. Dubbeldam, S. Calero, T. Vlugt, R. Krishna, T. Maesen, E. Beerdsen, B. Smit, *Phys. Rev. Lett.* **2004**, *93*, 088302.
[69] D. P. Cao, J. H. Lan, W. C. Wang, B. Smit, *Angew. Chem. Int. Ed.* **2009**, *48*, 4730; *Angew. Chem.* **2009**, *121*, 4824.
[70] Y. Y. Sun, K. Lee, Y.-H. Kim, S. B. Zhang, *Appl. Phys. Lett.* **2009**, *95*, 033109.
[71] R. Babarao, M. Eddaoudi, J. W. Jiang, *Langmuir* **2010**, *26*, 11196.
[72] M. Fischer, F. Hoffmann, M. Froba, *Colloids Surf. A* **2010**, *357*, 35 – 42.
[73] A. Kuc, T. Heine, G. Seifert, H. A. Duarte, *Theor. Chem. Acc.* **2008**, *120*, 543 – 550.
[74] Q. Min Wang, D. M. Shen, M. Bulow, M. L. Lau, S. G. Deng, F. R. Fitch, N. O. Lemcoff, J. Semanscin, *Microporous Mesoporous Mater.* **2002**, *55*, 217 – 230.
[75] L. Hamon, E. Jolimatre, G. D. Pirngruber, *Ind. Eng. Chem. Res.* **2010**, *49*, 74977503.
[76] B. Li, Z. Zhang, Y. Li, K. Yao, Y. Zhu, Z. Deng, F. Yang, X. Zhou, G. Li, H. Wu, N. Nijem, J. Chabal, Z. Lai, Y. Han, Z. Shi, S. Feng, J. Li, *Angew. Chem. Int. Ed.* **2012**, *51*, 1412 – 1415; *Angew. Chem.* **2012**, *124*, 1441 – 1444.
[77] A. R. Millward, O. M. Yaghi, *J. Am. Chem. Soc.* **2005**, *127*, 17998 – 17999.
[78] D. C. Dietzel, R. E. Johnsen, H. Fjellvag, S. Bordiga, E. Groppo, S. Chavanc, R. Blom, *Chem. Commun.* **2008**, 5125 – 5127.
[79] D. C. Dietzel, V. Besikiotis, R. Blom, *J. Mater. Chem.* **2009**, *19*, 7362 – 7370.
[80] D. Britt, H. B. Furukawa, T. G. Wang, O. M. Y. Glover, *Proc. Natl. Acad. Sci. USA* **2009**, *106*, 20637.
[81] J. A. Mason, K. Sumida, Z. R. Herm, R. Krishna, J. R. Long, *Energy Environ. Sci.* **2011**, *4*, 3030 – 3040.
[82] Z. R. Herm, J. A. Swisher, B. Smit, R. Krishna, J. R. Long, *J. Am. Chem. Soc.* **2011**, *133*, 5664 – 5667.
[83] Q. Yang, C. Xue, C. Zhong, J.-F. Chen, *AIChE J.* **2007**, *53*, 283.
[84] Y. Belmabkhout, G. Pirngruber, E. Jolimaitre, A. Methivier, *Adsorption* **2007**, *13*, 341 – 349.
[85] Y. F. Chen, A. Nalaparaju, M. Eddaoudi, J. W. Jiang, *Langmuir* **2012**, *28*, 3903 – 3910.
[86] R. Babarao, J. Jiang, *Energy Environ. Sci.* **2009**, *2*, 1088.
[87] J. Jiang, *AIChE J.* **2009**, *55*, 2422.
[88] S. Couck, J. F. M. Denayer, G.-V. Baron, T. Remy, J. Gascon, F. Kapteijn, *J. Am. Chem. Soc.* **2009**, *131*, 6326 – 6327.
[89] H. X. Deng, C. J. Doonan, H. Furukawa, R. B. Ferreira, J. Towne, C. B. Knobler, B. Wang, O. M. Yaghi, *Science* **2010**, *327*, 846 – 850.
[90] T. M. McDonald, D. D. M. R. Krishna, J. R. Long, *Chem. Sci.* **2011**, *2*, 2022 – 2028.
[91] Y. Liu, J. Liu, M. Chang, C. Zheng, *J. Phys. Chem. C* **2012**, *116*, 16985 – 16991.

© 2015 Wiley-VCH Verlag GmbH & Co. KGaA, Weinheim

[92] A. Torrisi, C. Mellot-Draznieks, R. G. Bell, *J. Chem. Phys.* **2010**, *132*, 044705.
[93] A. O. Yazaydin, A. I. Benin, S. A. Faheem, P. Jakubczak, J. J. Low, R. R. Willis, R. Q. Snurr, *Chem. Mater.* **2009**, *21*, 1425 – 1430.
[94] Z. Zhang, Z.-Z. Yao, S. Xiang, B. Chen, *Energy Environ. Sci.* **2014**, *7*, 2868 – 2899.
[95] N. Burtch, H. Jasuja, D. Dubbeldam, K. Walton, *J. Am. Chem. Soc.* **2013**, *135*, 7172 – 7180.
[96] J. Park, J. Kim, S. Han, Y. Jung, *J. Phys. Chem. Lett.* **2012**, *3*, 826 – 829.
[97] A. Yazaydin, R. Snurr, T. Park, K. Koh, J. Liu, M. LeVan, A. Benin, P. Jakubczak, M. L. D. Galloway, J. Low, R. Willis, *J. Am. Chem. Soc.* **2009**, *131*, 18198 – 18199.
[98] C. Wilmer, R. Snurr, *Chem. Eng. J.* **2011**, *171*, 775 – 781.
[99] R. Krishna, *Microporous Mesoporous Mater.* **2014**, *185*, 30 – 50.
[100] R. S. Pillai, S. A. Peter, R. V. Jasra, *Langmuir* **2007**, *23*, 8899.
[101] S. U. Rege, R. T. Yang, *Ind. Eng. Chem. Res.* **1997**, *36*, 5358.
[102] Y. Li, R. T. Yang, *Langmuir* **2007**, *23*, 12937 – 12944.
[103] X. Lin, A. J. Blake, C. Wilson, X. Z. Sun, N. R. Champness, M. W. George, P. Hubberstey, R. Mokaya, M. Schroedes, *J. Am. Chem. Soc.* **2006**, *128*, 10745 – 10753.
[104] R. Matsuda, R. Kitaura, S. Kitagawa, Y. Kubota, R. Belosludov, T. C. Kobayashi, H. Sakamota, T. Chiba, M. Takata, T. Kawazoe, Y. Mita, *Nature* **2005**, *436*, 238.
[105] J. W. Yoon, I. T. Jang, K. Y. Lee, Y. K. Hwang, J. S. Chang, *Bull. Korean Chem. Soc.* **2010**, *31*, 220.
[106] N. Lamia, M. Jorge, M. A. Granat, F. A. A. Paz, H. Chevreau, A. E. Rodrigues, *Chem. Eng. Sci.* **2009**, *64*, 3246.
[107] M. Hartmann, S. Kunz, D. Himsl, O. Tangermann, S. Ernst, A. Wagener, *Langmuir* **2008**, *24*, 8634.
[108] S. Han, W. Goddard III, *J. Am. Chem. Soc.* **2007**, *129*, 8422 – 8423.
[109] K. Mulfort, J. Hupp, *J. Am. Chem. Soc.* **2007**, *129*, 9604 – 9605.
[110] E. Klontzas, A. Mavrandonakis, E. Tylianakis, G. Froudakis, *Nano Lett.* **2008**, *8*, 1572 – 1576.
[111] T. Vlugt, R. Krishna, B. Smit, *J. Phys. Chem. B* **1999**, *103*, 1102 – 1118.
[112] N. Chen, W. Garwood, F. Dwyer, *Shape Selective Catalysis in Industrial Applications*, Marcel Dekker, New York, **1989**.
[113] R. Krishna, B. Smit, S. Calero, *Chem. Soc. Rev.* **2002**, *31*, 185 – 194.
[114] R. Krishna, *Phys. Chem. Chem. Phys.* **2015**, *17*, 39 – 59.
[115] B. Smit, T. Maesen, *Chem. Rev.* **2008**, *108*, 4125 – 4184.
[116] B. Smit, T. Maesen, *Nature* **2008**, *451*, 671 – 678.
[117] J. Talbot, *AIChE J.* **1997**, *43*, 2471 – 2478.
[118] T. Vlugt, W. Zhu, F. Kapteijn, J. Moulijn, B. Smit, R. Krishna, *J. Am. Chem. Soc.* **1998**, *120*, 5599 – 5600.
[119] Z. Du, G. Manos, T. Vlugt, B. Smit, *AIChE J.* **1998**, *44*, 1756 – 1764.
[120] J. van de Graaf, F. Kapteijn, J. A. Moulijn, *AIChE J.* **1999**, *45*, 497.
[121] F. Kapteijn, J. Moulijn, R. Krishna, *Chem. Eng. Sci.* **2000**, *55*, 2923.
[122] R. Krishna, D. Paschecк, *Phys. Chem. Chem. Phys.* **2001**, *3*, 453.
[123] R. Rohrbaugh, P. Jurs, *Anal. Chim. Acta* **1987**, *199*, 99 – 109.
[124] Accelrys, Materials Studio, Accelrys. 2001 – 2007 Accelrys Software Inc., http://accelrys.com/products/materials-studio/index.html.
[125] B. Smit, R. Krishna, *Handbook of Zeolite Science and Technology*, Marcel Dekker, Inc. New York, **2003**, pp. 317 – 340.
[126] M. Schenk, S. Vidal, T. Vlugt, B. Smit, R. Krishna, *Langmuir* **2001**, *17*, 1558 – 1570.
[127] J. M. van Baten, R. Krishna, *Microporous Mesoporous Mater.* **2005**, *84*, 179 – 191.
[128] J. Jiang, S. Sandler, *J. Chem. Phys.* **2006**, *124*, 024717.
[129] D. Santilli, T. V. Harris, S. Zones, *Microporous Mater.* **1993**, *1*, 329 – 341.
[130] D. Santilli, *J. Catal.* **1986**, *99*, 335 – 341.
[131] C. Cavalcante Jr., D. M. Ruthven, *Ind. Eng. Chem. Res.* **1995**, *34*, 177 – 184.
[132] H. Funke, A. Argo, J. Falconer, R. Noble, *Ind. Eng. Chem. Res.* **1997**, *36*, 137 – 143.
[133] R. N. C. J. Gump, J. Falconer, *Ind. Eng. Chem. Res.* **1999**, *38*, 2775 – 2781.
[134] R. Krishna, B. Smit, *Chem. Innovation* **2001**, *31*, 27 – 33.
[135] S. Calero, B. Smit, R. Krishna, *J. Catal.* **2001**, *202*, 395 – 401.
[136] S. Calero, B. Smit, R. Krishna, *Phys. Chem. Chem. Phys.* **2001**, *3*, 4390 – 4398.
[137] C. Baerlocher, B. McCusker, D. Olson, *Atlas of Zeolite Framework Types*, 6th ed., Elsevier, Amsterdam, **2007**.
[138] L. Alaerts, C. Kirschhock, M. Maes, M. van der Veen, V. Finsy, A. Depla, J. Martens, G. Baron, P. Jacobs, J. Denayer, D. de Vos, *Angew. Chem. Int. Ed.* **2007**, *46*, 4293 – 4297; *Angew. Chem.* **2007**, *119*, 4371 – 4375.
[139] V. Finsy, H. Verelst, L. Alaerts, D. De Vos, P. A. Jacobs, G. V. Baron, J. Denayer, *J. Am. Chem. Soc.* **2008**, *130*, 7110 – 7118.
[140] J. Castillo, T. Vlugt, S. Calero, *J. Phys. Chem. C* **2009**, *113*, 20869 – 20874.
[141] R. Krishna, J. van Baten, *Phys. Chem. Chem. Phys.* **2011**, *13*, 10593 – 10616.
[142] A. Torres-Knoop, R. Krishna, D. Dubbeldam, *Angew. Chem. Int. Ed.* **2014**, *53*, 7774 – 7778; *Angew. Chem.* **2014**, *126*, 7908 – 7912.
[143] A. Torres-Knoop, J. Heinen, R. Krishna, D. Dubbeldam, *Langmuir* **2015**, *31*, 3771 – 3778.
[144] A. Torres-Knoop, S. Balestra, R. Krishna, S. Calero, D. Dubbeldam, *ChemPhysChem* **2015**, *16*, 532 – 535.
[145] D. Dubbeldam, R. Krishna, S. Calero, O. Yazaydin, *Angew. Chem. Int. Ed.* **2012**, *51*, 11867 – 11871; *Angew. Chem.* **2012**, *124*, 12037 – 12041.
[146] B. Severson, R. Snurr, *J. Chem. Phys.* **2007**, *126*, 134708.
[147] F. Lahoz-Martín, A. Martin-Calvo, S. Calero, *J. Phys. Chem. C* **2014**, *118*, 13126 – 13136.
[148] M. Allen, D. Tildesley, *Computer Simulation of Liquids*, Clarendon Press, Oxford, **1987**.
[149] D. Frenkel, B. Smit, *Understanding Molecular Simulation*, 2nd ed., Academic Press, London, **2002**.
[150] D. Dubbeldam, A. Torres-Knoop, K. Walton, *Mol. Simul.* **2013**, *39*, 1253 – 1292.
[151] M. Martin, J. Siepmann, *J. Phys. Chem. B* **1998**, *102*, 2569 – 2577.
[152] W. Jorgensen, D. Maxwell, J. Tirado-Rives, *J. Am. Chem. Soc.* **1996**, *118*, 11225 – 11236.
[153] P. Bai, M. Tsapatsis, J. Siepmann, *J. Phys. Chem. C* **2013**, *117*, 24375 – 24387.
[154] S. Mayo, B. Olafson, W. Goddard, *J. Phys. Chem.* **1990**, *94*, 8897 – 8909.
[155] A. Rappe, C. Casewit, K. Colwell, W. Goddard, W. Skiff, *J. Am. Chem. Soc.* **1992**, *114*, 10024 – 10035.
[156] R. Krishna, J. Long, *J. Phys. Chem. C* **2011**, *115*, 12941 – 12950.

Received: March 4, 2015
Revised: April 11, 2015
Published online on May 20, 2015

© 2015 Wiley-VCH Verlag GmbH & Co. KGaA, Weinheim